Doctoral Thesis

Numerical Simulation on Thermal Impact of Open-Loop Geothermal Heat Pump System in the Alluvial Fan of the Nagara River, Gifu City, Japan

Randa Permanda

1193921107

Gifu University

Graduate School of Engineering Doctor's Program

Department of Engineering Science

March 2023

Table of Contents

ABSTRACT

The open-loop Geothermal Heat Pump (GHP) system uses thermal energy of groundwater for heating and cooling of building. It is necessary to assess the thermal effect of injected groundwater after heat exchange in the system. Gifu city is located on the alluvial fan of the Nagara River. Alluvial fan is a good area to install open-loop GHP systems due to shallower aquifer, faster groundwater flow, fewer land subsidence risk, and so on. The alluvial fan of the Nagara River is influenced by the recharging from river to underground. Because of this circumstance, natural change of river water temperature and lateral groundwater flow has an impact on groundwater temperature. Natural change of groundwater temperature in the alluvial fan of the Nagara River, central Japan are greatly affected near the apex of the alluvial fan. The fluctuating groundwater temperature not only near the surface but also in the aquifer. This natural change of groundwater temperature gets smaller towards the toe of the alluvial fan. It is confirmed by the phase difference of ground temperature to river temperature increasing from north to south on the southern side of the river. Groundwater flow velocity is faster in areas less than 4 km from the recharge area, and slower further than 4 km. Understanding the effect of natural change of groundwater temperature in this area on thermal impact of utilizing open-loop GHP system is very important to study to prevent conflicts with adjacent geothermal heat pump systems and maintain their sustainability. The purpose of this research is to understand the thermal impact of groundwater extraction and injection using an open-loop GHP system varied by two different local underground conditions on alluvial fan of the Nagara River: 1. local model 1 with fast groundwater flow velocity and natural change of groundwater temperature, 2. local model 2 with slow groundwater flow velocity and limited natural change of groundwater temperature.

There are 2 different scales of model, a regional scale and local scale are constructed in the alluvial fan of the Nagara River. The FEFLOW program were used to create a regional 3D model of groundwater flow with heat transport. The regional scale model is constructed using hydrological and geological data. The local scale model is applied as a small part of

the regional model with finer mesh with applying the open-loop GHP system. The operation of open-loop GHP was applied for heating from January to March, and cooling from July to September. For the cooling and heating periods of the open-loop GHP system, the groundwater was returned to the injection well with three variant values: 0, 5, and 10 °C higher and lower than the original groundwater temperature. Pumping and injecting flow rates were 0 m^3 /s (non-active), 3.33×10^{-3} m^3/s, 6.67×10^{-3} m^3/s, 1.67×10^{-2} m^3/s, and 3.33×10^{-2} m^3/s.

The regional simulation results of groundwater flow and heat transports were confirmed with hydraulic head and groundwater temperatures from the measured data by Ohtani et al., (2015). The calculated results of the regional simulation were almost consistent with the measured ones in southern part. The calculated results are well correlated according to distribution of hydraulic head and groundwater temperatures, annual groundwater temperature change, phase difference, temperature fluctuation between maximum and minimum, and average groundwater temperature with the measured data. In contrast to the southern part, comparison between calculated and measured groundwater temperature data shows no similar patterns in the northern part. There is no relationship between lateral flow from the recharge area and groundwater temperature distribution in the northern side. However, in general, the regional simulation has well-represented groundwater flow and heat transport in southern part, which are influenced by natural change and lateral groundwater flow in the alluvial fan of the Nagara River area. The southern region can be used for local simulation of the model.

The local simulation results showed that local model 1 with a rapid groundwater flow velocity and natural change of groundwater temperature had a lower thermal impact than local model 2 with a slow groundwater flow velocity and limited natural change of groundwater temperature. In the local model 1, groundwater temperature is lower in the summer and higher in the winter during operation due to the existence of fast groundwater flow velocity and natural temperature change. As a result, a slight slope of groundwater temperature change was found in the heating and cooling periods in local model 1. As for

local model 2, thermal change continued to increase until the end of the period due to the small influence of natural changes in the groundwater. In local model 1, the thermal change due to open-loop system operation decreases faster than local model 2 due to faster groundwater flow as we can see at the same distance of 100m. Furthermore, the thermal impact of local model 1 recovers faster than model 2. The groundwater temperature in local model 1 is returned to natural condition after 90 days of heating and cooling. Meanwhile, thermal plumes are appeared downstream at a distance of 450 m in local model 2. This situation makes this area suitable for regional thermal energy storage as the groundwater temperature in this area is slightly cooler in summer and slightly warmer in winter.

Keywords: open-loop geothermal heat pump, thermal impact, FE FLOW

List of Figures

List of Tables

CHAPTER 1: INTRODUCTION

1.1 BACKGROUND OF PROBLEM

The environmental impact of global warming induced by the use of fossil fuels has increased awareness of the renewable energy systems. As a result, the usage of geothermal heat pumps for heating and cooling systems in residential and commercial buildings has increased. Geothermal Heat Pumps (GHP) or Ground Source Heat Pumps (GSHP) provide enormous prospects for energy efficiency as well as considerable reductions in CO_2 emissions, global warming impacts, and pollution (Lund et al., 2011; Sanner et al., 2003; Bayer et al., 2012). GHP is a system that generates heat by utilizing various types of heat existing on the earth. Since the temperature of underground and groundwater is constant throughout the year, the temperature is lower in summer and higher in winter relative to the outside air, so GHP can be used to create more efficient heating and cooling than air-source heat pumps (Figure 1). In addition, since GHP do not involve combustion, they can produce heat energy with minimal CO_2 emissions (Rivoire et al., 2018).

GHP systems are classified as closed-loop and open-loop systems (Figure 2). Closed-loop system circulates an antifreeze fluid through a pipe that is buried underground. Closed loop design is classified into four types: vertical closed loop, horizontal closed loop, closed spiral loop, and closed pond loop. An open-loop system connects directly with the groundwater. Open-loop system uses groundwater as a direct heat transfer medium. The water is extracted and passed through the heat exchanger of the heat pump, and then discharged back to the aquifer. Closed-loop system extract heat from underground with inserted pipes in boreholes. The advantage of this system is free maintenance, but it is costly due to many boreholes. In other side, open-loop system extract groundwater to transfer a heat. It has advantage for the area that has abundance of groundwater, but it needs extra maintenance depending on water chemistry.

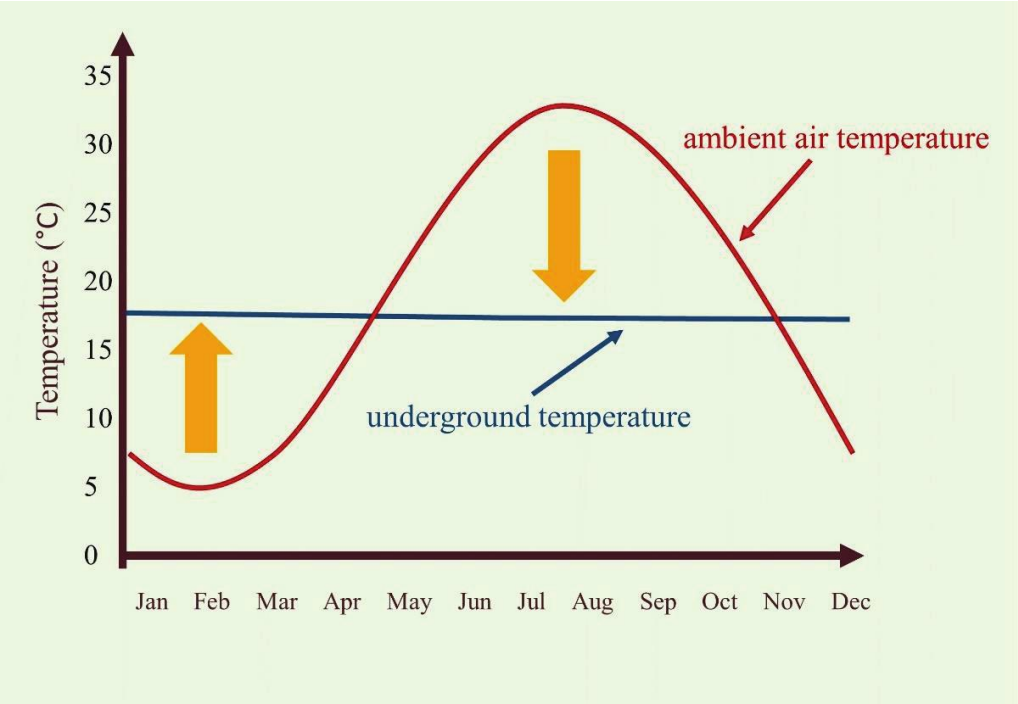

Figure 1. Ambient air temperature and underground temperature throughout the year

A geothermal heat pump system's three basic components are the heat pump, the ground loop, and the distribution system. The heat pump is the core of the geothermal heat pump system. It delivers heat from the ground loop to the compressor and then to the distribution system. A geothermal heat pump system includes a ground loop, which absorbs heat from the earth or groundwater and delivers it to the heat pump. Through a network of pipes, the distribution system transports and distributes the heat collected by the heat pump (especially in the condenser) to the building. Their efficiency is heavily impacted by the heating and cooling load, as well as the heat pump design elements (such as compressor efficiency and temperature control). Indicator of energy efficiency: COP (Coefficient of Performance) is a numerical value that represents how much thermal capacity (kW) can be extracted per 1 kW of electric power consumption. The greater the value, the better the performance in terms of energy savings.

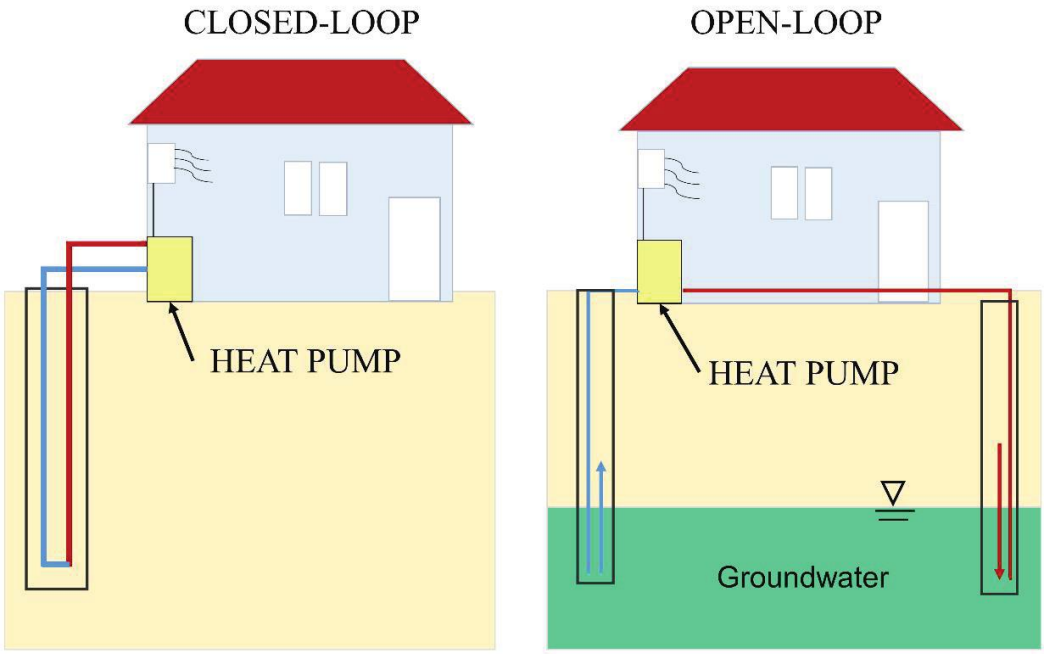

Figure 2. Types of geothermal heat pumps, closed-loop system (left), open-loop system (right)

The use of GHP systems in Japan has increased since the World Geothermal Congress in 2000. The Ministry of Environment (MoE) released statistics on GHP systems in 2019. Between 1981 and 2017, there were 2,662 facilities that used GHPs, including 2,314 closed-loop, 327 open-loop, and 21 that used both. The government recently recognized the benefits of using shallow geothermal energy for cooling and heating in terms of energy savings and avoiding additional CO_2 emissions. However, the quantity of installations remains quite low. Although the number of geothermal heat pumps installations in Japan are still relatively low, there is a noticeable number increasing every year. It is clear that heating and cooling space is essential in most parts of Japan (Yasukawa and Takasugi, 2003).

Some residential areas in Japan are located on alluvial deposits, which generally occur with rapid groundwater flow. Open-loop GHP systems, on the other hand, are not always feasible. Due to serious subsidence problems in the past, groundwater extraction is strictly prohibited in many large urban areas. Thus, closed-loop systems are more common than

open-loop systems in Japan. Although open-loop GHP systems account for only a small proportion of all GHP utilizations in Japan, the demand for open-loop geothermal heat pump applications in areas which is not prohibited by prefectural regulations is likely to grow. This is because open-loop systems are less costly than closed-loop systems and more practical.

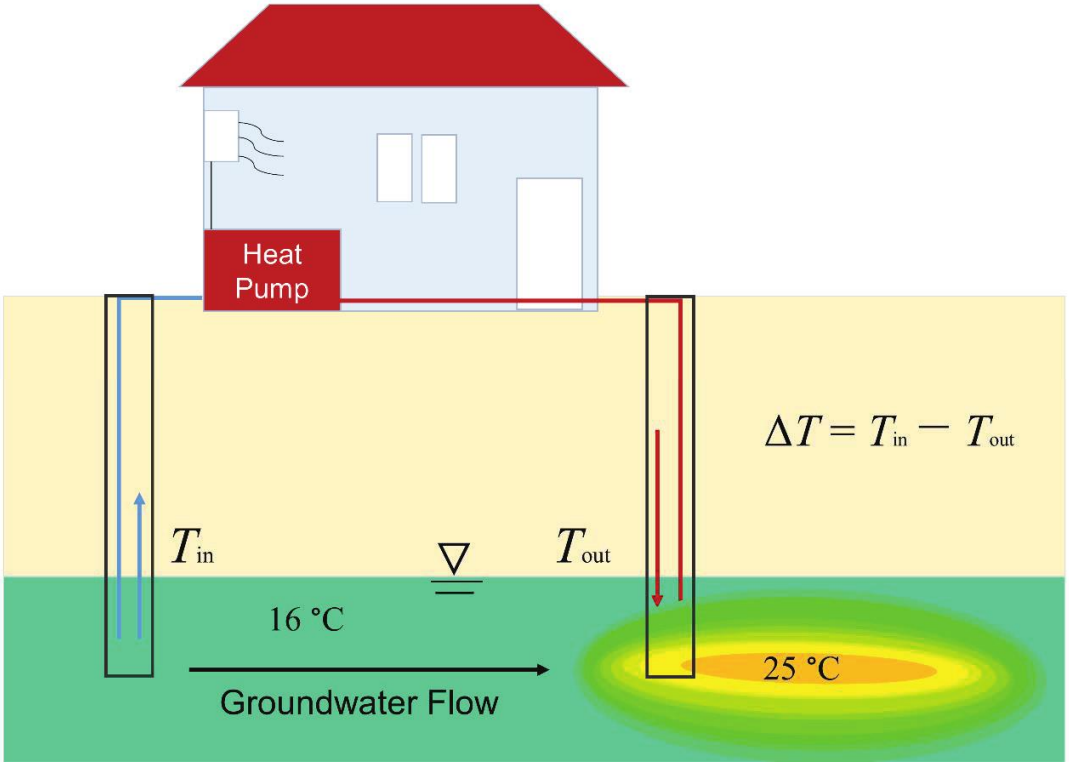

Figure 3. Schematic image of an open-loop geothermal heat pump system

This development puts more pressure on natural resources like groundwater, and there is increasing concern about the long-term sustainability of such extraction-injection (open-loop) systems and their impact on the thermal change of the aquifer (Figure 3). Groundwater extraction and injection caused thermal plumes in cooled and warmed groundwater, which spread throughout the subsurface environment. Depending on downstream aquifer usage, the plumes may be regarded as environmental damage. A thermal plume, for example, could negatively effects groundwater use downstream or affect the well system's sustainability via thermal feedback. However, effect of thermal energy discharge to the aquifer only give small threat on groundwater quality and groundwater ecosystem (Bonte et al., 2011; Brielmann et

al., 2009; Bulté, M.; Duren, T.; Bouhon, O.; Petitclerc, E.; Agniel, M.; Dassargues, 2021; Sommer et al., 2014).

A few researchers have examined into the environmental concerns that are caused using geothermal heat pumps. Meng et al. (2019) was assessed the thermal impacts and long-term sustainability of intensive domestic geothermal use. It was found that downstream installations showed a greater decrease in subsurface temperature and therefore reduced heat pump efficiency. He suggested that when planning GHP installations, site-specific groundwater flow parameters should be taken into account. Freedman et al. (2012) analyzed the possible thermal impact of GHP operation on upgradient extraction wells and the Columbia River. Low pumping rates not only save cost, but also reduce the possibility of thermal contamination at extraction wells. Groundwater discharges to the Columbia River would have minimal thermal impact downstream. Lo Russo et al. (2014) evaluated the Thermal Affected Zone (TAZ) that developed around the injection well with using average daily, monthly, and seasonal energetic equivalents flow rate and injection temperature. The use of hourly, daily, or monthly average injection flow rate and temperature data resulted in high-quality simulation results. In contrast, using seasonal average values did not yield accurate TAZ estimations. Casasso and Sethi (2015) performed thermal recycling evaluation between injection and extraction well using the numerical flow and heat transport simulation. The implemented mathematical models can be used for the design of small GHP with conservative parameter values.

The increasing demand of GHP system raised a question on the effect of their thermal performance. Thermal interference can be avoided with proper well spacing. However, oversizing well spacing may limit the number of systems that may be implemented in a region and reduce the potential for GHP system. The effect on groundwater temperature in the surrounding region is determined by the flow rate and temperature differential of water injected into the aquifer, as well as the aquifer's natural velocity and subsurface thermal dispersivity. If the thermal change reaches the extraction well, the temperature distribution in the aquifer has an impact on heat pump efficiency. As a result, the appropriate location of

the groundwater extraction-injection system must be determined early on by modeling of thermal impact in groundwater flow and subsurface heat transfer (Russo et al., 2011). Pophillat et al. (2020) investigated the effect of groundwater velocity, longitudinal and transverse dispersivity coefficients, and energy load parameters on the long-term thermal impact of variable injection. Piga et al. (2017) performed a numerical simulation to assess the thermal impact of an open-loop system of a GHP, comparing rigorous to simplified models. These previous studies implied that, in addition to the pumping rate and water injected temperature, the thermal impact is strongly influenced by subsurface conditions, such as hydraulic conductivity and thermal subsurface parameters.

Several studies have been conducted to investigate the feasibility of the GHP system in various regions of Japan. Fujii et al. (2007) developed suitability maps for installation of GHP system in the Chikushi Plain, western Japan. Shrestha et al. (2015) assessed the potential use of GHP system in regional scale in Tsugaru Plain, Japan. A potential map can be used to identify appropriate areas for space heating. The suitability maps of heat exchange rate help in the optimization of GHP system site and design. According to Nam et al. (2008) the heat extraction and injection rates of the heat exchanger must be precisely predicted for the design of a GHP system. Okano et al., (2021) examined geochemical study from open-loop GHP system in Akaiwa City and the northeastern part of Okayama City. Okano et al., (2021) concluded open-loop GHP can be used. However, for groundwater with high iron concentrations, closed-loop GHP system is recommended.

There are no laws or suggestions in most countries regarding temperature restrictions for the thermal use of groundwater and the subsurface (Haehnlein et al., 2010). In many countries, GHP is underutilized when compared to other renewable energy sources. Because of the lack of expertise, there is no acknowledged requirement for limits. Regulation of minimal distance between GHP installations can reduce possible thermal impact on neighboring properties or buildings. Environmental regulations can help control and avoid catastrophic effects on the environment and future generations.

1.2 PROBLEM FORMULATION

We need model to understand the processes and make them predictable. The modeling of flow and heat transport processes in porous and fractured media comprises at least three major aspects: conceptual, numerical, and software/application. Conceptual model describes the components of the system, the physicochemical and physical phenomena, and the relevant characteristics of the medium in which they take place. The numerical model uses numerical algorithms and discrete solution methods. Due to its variable geometries, unstructured meshes, robustness, and mathematical foundation, FEM (finite element method) is the most general and powerful method (Diersch, 2014). The final step is to implement computational models using appropriately established simulation software. In this study, DHI FEFLOW (Finite Element subsurface FLOW and transport system) version 7.0 was used for simulating groundwater flow and heat transport modeling. FEFLOW is an interactive groundwater modeling system for three-dimensional and two-dimensional in subsurface water environments with or without one or multiple free surfaces. FEFLOW can be efficiently used to perform the groundwater flow and heat transport simulation of an open-loop geothermal installation. FEFLOW can assist in the prediction of a GHP system's operational performance, the effects on other potential groundwater users, and the simulation of long-term thermal interference effects.

The FEFLOW model does not require a programming language because it performs its own calculations. FEFLOW users can concentrate on concept rather than programming language complexities (Figure 4). Supermesh can be composed of an arbitrary number of polygons, lines and points. Material information is assigned to finite elements during model parametrization. The process variables (hydraulic head, mass concentration, temperature, mean groundwater age, mean lifetime expectancy, and exit probability concentration) are solved using a system of equations based on each node of the finite-element mesh. Simulation results can be stored in two different formats: a reduced results file (*.dar) and a full simulation record (*.dac).

Figure 4. Workflow of conceptual modelling

The use of shallow geothermal energy highly depends on the local condition. The temperature of underground has site-specific condition. The hydrogeological subsurface simulations must match as closely as possible the actual conditions to correctly compute the thermal change by operation of open-loop system. In this paper, we model the regional groundwater flow and heat transport system in the alluvial fan of the Nagara River in Gifu, central Japan. This is an example of an alluvial fan area influenced by infiltrating surface water from a river. Underground temperatures near the apex of an alluvial fan are influenced by seasonal temperature changes and lateral groundwater flow. The velocity of ground water flow is faster in the area less than 4 km from the recharge area, and slower more than 4 km. River water enters the aquifer, influencing the temperature of the groundwater. This influence causes the zone whose temperatures are cooler than the Nagara River in the summer, but warmer than the river water in the winter. Temperature fluctuations, however, decrease as one moves from upstream of the Nagara river to the downstream side. This influence is evident from observation wells that were monitored at monthly intervals across the Gifu city area from May 2013 to May 2014 (Ohtani et al., 2015).

There has been no study of the thermal environmental impact of an open-loop GHP system in alluvial fan areas with natural temperature changes due to groundwater flow. Most studies have examined the thermal impacts and sustainability of intensive shallow geothermal utilization at alluvial and glaciofluvial deposits, with no significant vertical temperature variation in groundwater. This study was performed to understand the thermal environmental impact of an open-loop GHP system in areas with natural temperature changes in groundwater. GHP systems have the potential to be an economical, sustainable, and environmentally friendly heating and cooling options, but they need to be carefully planned.

1.3. OBJECTIVE

We aimed to see how the thermal impact of groundwater extraction and injection using an open-loop GHP system varied in two different local locations with different underground conditions: 1. local model 1 with fast groundwater flow velocity and natural change of groundwater temperature, 2. local model 2 with slow groundwater flow velocity and limited natural change of groundwater temperature. The regional simulation was performed to understand the patterns of regional groundwater flow and heat transport. The local simulation was performed to understand the thermal environmental impact accompanied by the operation of the open-loop GHP system on the 2 local models on the Nagara River alluvial fan.

CHAPTER 2: METHODOLOGY

2.1 BASIC THEORY

This chapter summarize some basic concept and definition of groundwater flow and heat transport (Wang and Manga, 2021).

Groundwater moves from levels of higher energy to levels of lower energy, so its energy level is essentially the result of elevation and pressure. Groundwater flow is driven by both the gradient of the pressure energy and the gravitational energy (elevation), which are conveniently combined into the hydraulic head h [m] in hydrogeology:

$$h = \frac{P}{\rho_f g} + z \tag{2.1}$$

where P [Pa] is fluid pressure, g [m/s^2] is gravity acceleration, ρ_f [kg/m^3] is fluid density and z [m] is elevation. The first term on the right of the equation is the pressure head, the second the elevation head.

The fundamental equation describing the flow of groundwater was described by Darcy (1856). Darcy's Law is an empirical equation that describes the flow of fluids through a porous medium. It was first introduced by Henry Darcy in 1856 and has since become a fundamental concept in hydrogeology, petroleum engineering, and other fields. Darcy law's states that the rate of flow through a porous medium is proportional to the loss of head and inversely proportional to the length of the flow path, or

$$v = K\frac{\nabla h}{\nabla l} = -Ki \tag{2.2}$$

where v is specific discharge or Darcy velocity (m/s); K is hydraulic conductivity (m/s); ∇h is head loss (m); ∇l is length of flow path (m); and i is the hydraulic gradient (-).

Darcy's law can alternatively be written as

$$Q = -K\frac{\nabla h}{\nabla l}A = -KiA \tag{2.3}$$

where Q is the volume rate of flow (m^3/s) and A is the cross-sectional area normal to flow direction (m^2).

The hydraulic conductivity K is a parameter depending on the properties of the porous medium and of the fluid. It is the flow rate per unit cross-sectional area under influence of a unit gradient. The hydraulic conductivity K differs from the permeability, k. The relation between two parameters is

$$K = k\frac{\rho g}{\mu} \tag{2.4}$$

where k is intrinsic permeability of the porous medium (m^2); ρ is density of fluid, i.e.: water (kg/m^3); g is the acceleration due to gravity (m/s^2); and μ is the dynamic viscosity of the fluid, i.e.: water (kg/m.s).

In using Darcy's law, it is important to know the range of validity. After all, Darcy (1856) conducted his experiments on sand samples in the laboratory. Darcy's law is valid for laminar flow, but it is not valid when the flow is turbulent, as may happen in cavernous limestone, or fractured basalt. If there is any doubt, the Reynolds number serves as criterion to distinguish between laminar and turbulent flow. The Reynolds number is expressed as

$$N_R = \rho\frac{vd}{\mu} \tag{2.5}$$

where d is a representative length dimension of the porous medium, usually taken as a mean grain diameter or a mean pore diameter (m).

Several experiments have shown that Darcy's law is valid for N_R <1 and does not create severe errors up to N_R = 10. This value represents an upper limit to the validity of Darcy's law. It should not be considered as unique limit, however because of turbulence arise gradually. At full turbulence, the head loss is not linear but is approximately the velocity squared. Fortunately, most groundwater flow occurs with N_R <1 so that Darcy's law applies. Only in exceptional situations, where the rock contains wide openings, or in the near vicinity of a pumped well, will the criterion of laminar flow remain unsatisfied and will Darcy's law then not be valid.

The well-flow equations presented are based on several assumptions; one of which is that aquifer and aquitards are homogeneous and isotropic. This means that the hydraulic conductivity is independent of where it is measured within the formation and also independent of direction of measurement.

Heat transport in groundwater systems occurs through both conduction and advection by fluid flow. The conductive transport is governed by Fourier's law

$$q_h = -K_h \cdot \nabla T \tag{2.6}$$

where q_h [W/m^2] is the heat flux by conduction, K_h [W/(m-K)] is the thermal conductivity tensor, and T $[K]$ is temperature. For saturated porous media, the average thermal conductivity may be estimated with

$$K_h = K_f^{\varphi} K_r^{1-\varphi} \tag{2.7}$$

where K_f and K_r are, respectively, the thermal conductivity of the pore fluid and the solid rock. At 25 °C, K_f is about 0.6 W/ (m K) so that the thermal conductivity of saturated porous rocks is dominated by the mineralogy.

Combining Fourier's law (2.6) with the conservation law for thermal energy, we obtain the differential equation for the thermal transport of heat by conduction

$$\rho c \frac{\partial T}{\partial t} = \nabla \cdot (K_h \cdot \nabla T) + Q_h \tag{2.8}$$

where ρ (kg/m^3) and c (J/(kg.K) are, respectively, the bulk density and specific heat of the aquifer, and Q_h (W/m^3) is a heat source (positive) or heat sink (negative) per unit volume. Takes the simplified form: If Q_h = 0 and the aquifers is uniform and isotropic (i.e., constant K_h), Eq. (2.8) takes the simplified form:

$$c\rho \frac{\partial T}{\partial t} = K_h \nabla^2 T \tag{2.9}$$

The product $c\rho$ for a porous rock with porosity φ may be estimated from the arithmetic mean of the solid and fluid components of the aquifer, i.e., $c\rho = \varphi\rho_f c_f + (1-\varphi)\rho_r c_r$, where c_f is the specific heat of the pore fluid and c_r that of the rock matrix.

Fluid flow can be effective at transporting heat. The amount of advective transport is proportional to the gradient of the thermal energy and the specific discharge. Hence heat transport in groundwater consists of both a conductive process and an advective process, and the governing equation becomes

$$\left[\varphi\rho_f\, c_f + (1-\varphi)\,\rho_r c_r\right]\frac{\partial T}{\partial t} = K_h\nabla^2\mathrm{T} - \rho_f \mathrm{c}_f \mathbf{q}\cdot\nabla\mathrm{T}, \qquad (2.10)$$

The specific discharge $\mathbf{q}$ in the equation couples groundwater flow to heat transport.

2.2 STUDY AREA

The study area is an alluvial fan of the Nagara River in Gifu city, Gifu Prefecture, central Japan, located on the Nobi Plain's margin. The Nobi Plain has an area of around 1,300 km^2. The Nobi Plain, which is tilted westward, is composed of Pliocene and Pleistocene gravel, sand, sandy clay, and clay. Three gravel layers that comprise the main aquifers are composed of riverbed gravel that was accumulated during glacial stages. Confining layers are composed of sandy-clay and clay deposited during inter-glacial stages. The regional groundwater flow system and surface warming from urbanization both have an impact on the thermal regime in the Nobi Plain. The Nobi Plain's annual mean air temperature has risen by about 2 ℃ over the last century. The annual mean air temperature has risen from 14 to 16 ℃ in the northern plain and from 14.5 to 16.5 ℃ in the southern plain (Uchida et.al, 2003).

The alluvial fan of the Nagara River is formed where the Nagara River emerges from the hill slopes. The Nagara River flows from the plain's north to the south. The study area is bounded on the north and northeast sides by mountain ranges, and on the west and south by the Gifu City border line (Figure 5 up). The mountains are composed of the Jurassic accretionary complex, which includes chert, sandstone, and shale. The underground formation of the alluvial fan consists of the Holocene gravel and silt deposits on the upper side and the Pleistocene gravel and sand strata beneath the Holocene beds (Figure 5 down).

Intercalate thin fine sand and silt layers that are only partially linked divide the aquifers into two parts. Precipitation and surface water continue to flow downhill in the alluvial fan region, recharging groundwater via permeable sand and gravel layers. River water recharges at the upstream area in the alluvial fan of the Nagara River.

Ohtani et al., (2015) conducted field surveys on groundwater level and subsurface temperature in the alluvial fan of the Nagara River. This study was conducted from May 2013 to May 2014. Temperature was measured in 17 boreholes with a length of 30 m. Measurements were made once a month with a thermistor thermometer at 1 m depth intervals. The underground temperature in the alluvial fan is influenced by rapid groundwater flow recharged from river. According to groundwater level measurements, the groundwater flow direction was generallly southwest in the southern side of the Nagara River. Changes in surface temperature have an impact on the temperature underground above a depth of 10 m, as can be seen on Figure 6 (left). Lateral groundwater flow influences the depth range of 10 m to 20 m. The depth below 20 m remains constant throughout the year. This suggests that aquifers are divided at a depth of 20 m. The existence of a thin sand layer at a depth of 20 m gives additional support to this (Figure 6 (right)). From 10 to 20 m depth, August and March have the lowest and highest temperatures, respectively. There is a six-month phase difference. Groundwater temperatures in the south are almost constant in all year (Figure 6 (right)). Nearly no phase difference exists. The difference in temperature between the lowest and highest measurements is 0.3 °C. The term “phase difference” refers to the time difference between outside air and underground temperature.

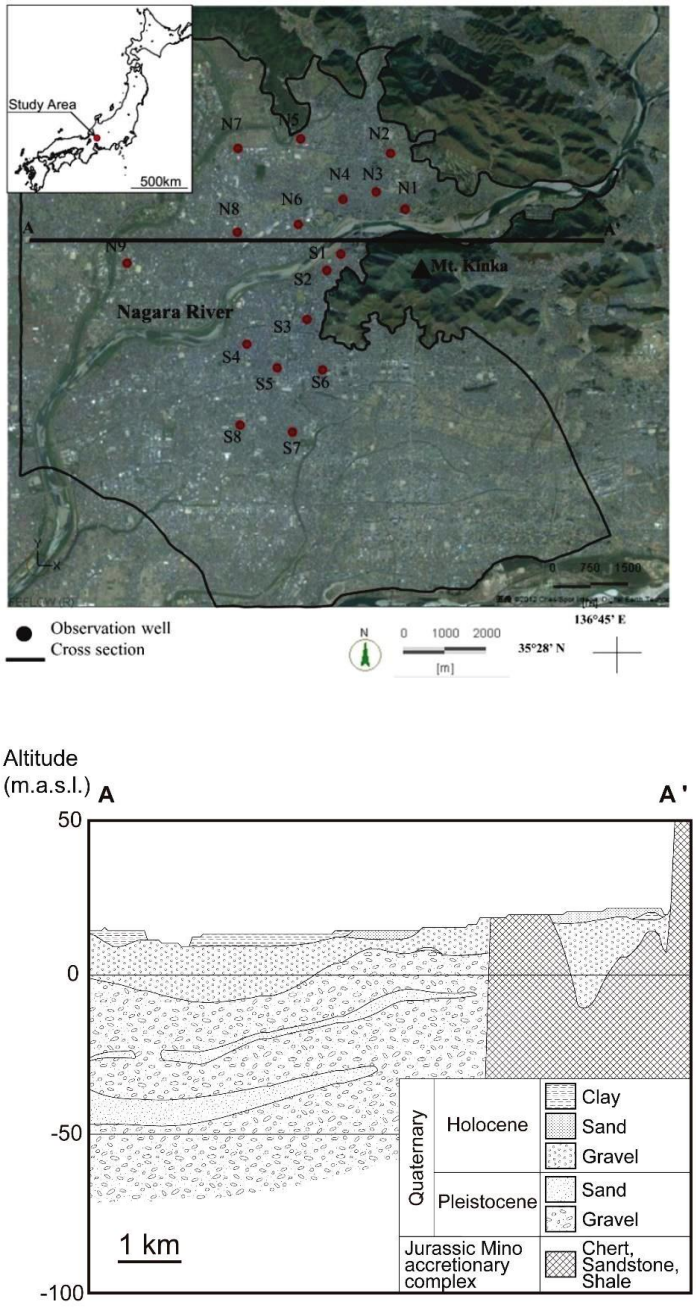

Figure 5. Study area (up) and geologic cross section (down) Alluvial fan of the Nagara River (red circles: observation wells, solid line: model boundary, line A-A': cross section)

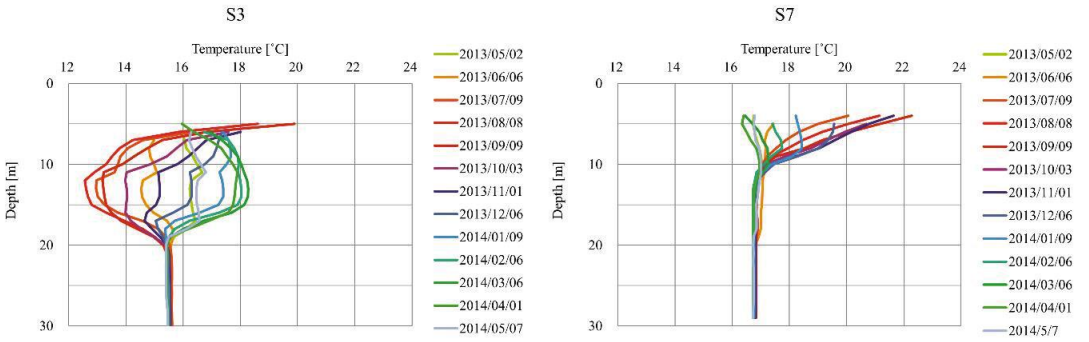

Figure 6. Vertical profiles of groundwater temperature of the observation wells in the alluvial fan of the Nagara River. Wells S3 (left) and S7 (right) are in the middle and toe of the alluvial fan, respectively (Ohtani et al., 2015).

The groundwater levels in the alluvial fan of the Nagara River as seen in Figure 7, increase from June to August and March to April. In the other months, groundwater levels remain stable. Groundwater level increases due to influence of high precipitation in summer compared than winter. Generally, the groundwater level is higher near the top of the alluvial fan, and lower near the base.

Natural changes in groundwater temperature in the alluvial fan of the Nagara River are greatly affected near the top of the alluvial fan. Groundwater temperature fluctuates not only near the surface but also within the aquifer. The groundwater temperature fluctuation between minimum and maximum becomes smaller toward the south. Figure 8 depicts the groundwater temperature at 15m depth. As can be seen, there is a phase difference between the Nagara River as a recharge area and the observation point. The farther away from the recharge area, the greater the phase difference. It is confirmed by the phase difference of ground temperature to river temperature increasing from north to south on the southern side of the river.

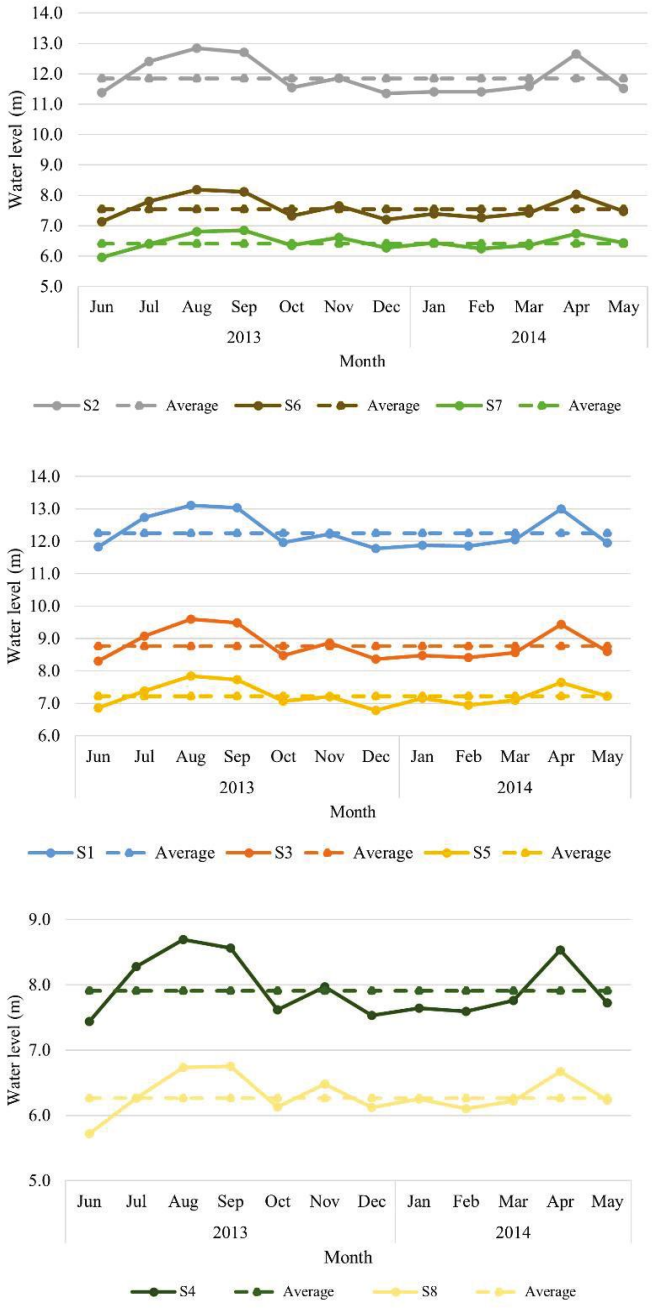

Figure 7. Groundwater level by observation points by Ohtani et al. (2015).

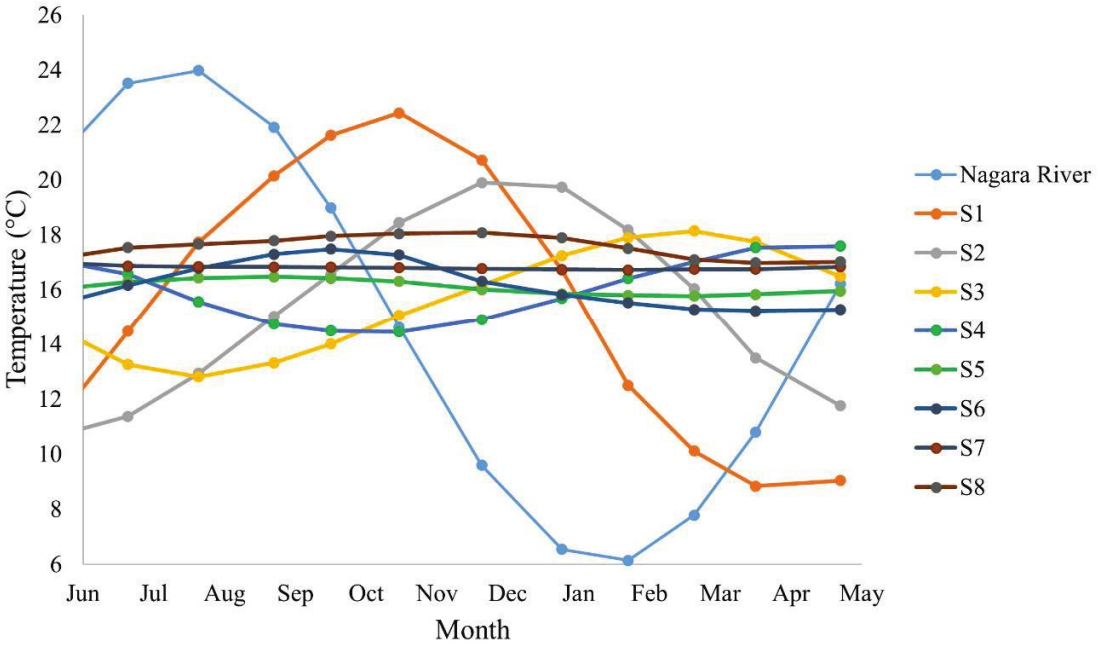

Figure 8. Groundwater temperature at 15m depth at observation points by Ohtani et al., (2015)

The Figure 9 showed the annual amount of pumping in the alluvial fan of the Nagara River. Groundwater extraction in Gifu city area is generally about 50.000 m^3/year with an area of about 600m × 800m. It was found 500.000 m^3/year, but it is very few. It is mostly concentrated in the southern, more urban areas. The pumping rate is assumed to affect the groundwater temperature distribution in the alluvial fan of the Nagara River. Therefore, in the groundwater flow simulation, the pumping rate is assigned to the model

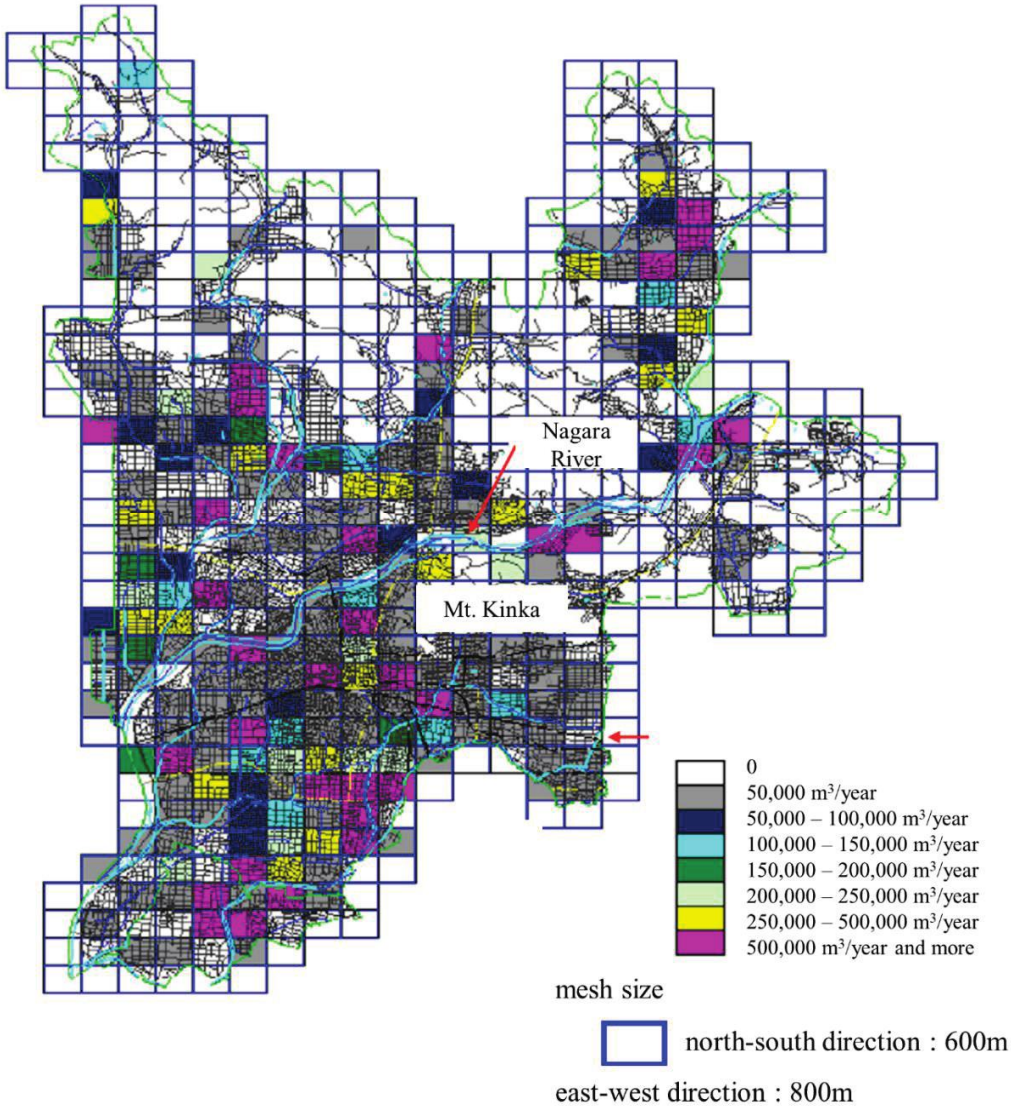

Figure 9. Reported groundwater extraction of Gifu City (Adapted from Gifu Prefecture, Gifu City, Teikoku Construction Consultant (2011), Report on feasibility study of geothermal heat pumps, 201p.

2.3 ANALYSIS MODEL

The groundwater flow system, as well as the distribution of subsurface temperature, must be thoroughly understood in order to assess the thermal impact of open-loop GHP system. A 3D regional simulation model was created for this purpose using the finite element software FEFLOW. The term "FEFLOW" stands for "finite element subsurface flow simulation system," which uses a multidimensional FEM to solve the flow, mass, and heat transport equations in porous and fractured media under complex geometric and parametric conditions, such as variable fluid density, variable saturation, free surfaces, multispecies reaction kinetics, non-isothermal flow, and multi diffusive (thermohaline) effects.

The model was created using pre-existing geological and hydrological data. The pre-existing geological columns and profile are used to build the model's geological layer. The pre-existing hydrological data such as groundwater table, groundwater temperature, and Gifu city groundwater extraction are applied. The geological data were given by Gifu City and Teikoku Engineering Consultants (2008), as was the hydrological survey by Ohtani *et al.* (2015). All of geological data were generated into an Excel file (*.xlsx) with columns: X, Y, elevation, and slice. The data files were connected to FEFLOW and attached to 3D layer configuration. Measurements of groundwater level and temperature will also be utilized to validate the simulation results.

The groundwater level measurement data by Ohtani et al. (2015) is limited only around of Gifu city area. Therefore, this measurement data cannot be used as a regional model boundary condition of hydraulic head. There are two groundwater levels distribution as shown in Figure 10 and Figure 11 which was based on groundwater level measurement on 195 observation points. Due to precipitation, the groundwater level on July 31-August 1, 2013, is higher than the groundwater level on February 20-21, 2014.

Based on the simulation result of fluid flow, the groundwater level on February 20-21, 2014 was relatively the similar to the average of groundwater level from measured by Ohtani et al., (2015). Therefore, we applied this value as the boundary condition of hydraulic head on regional model.

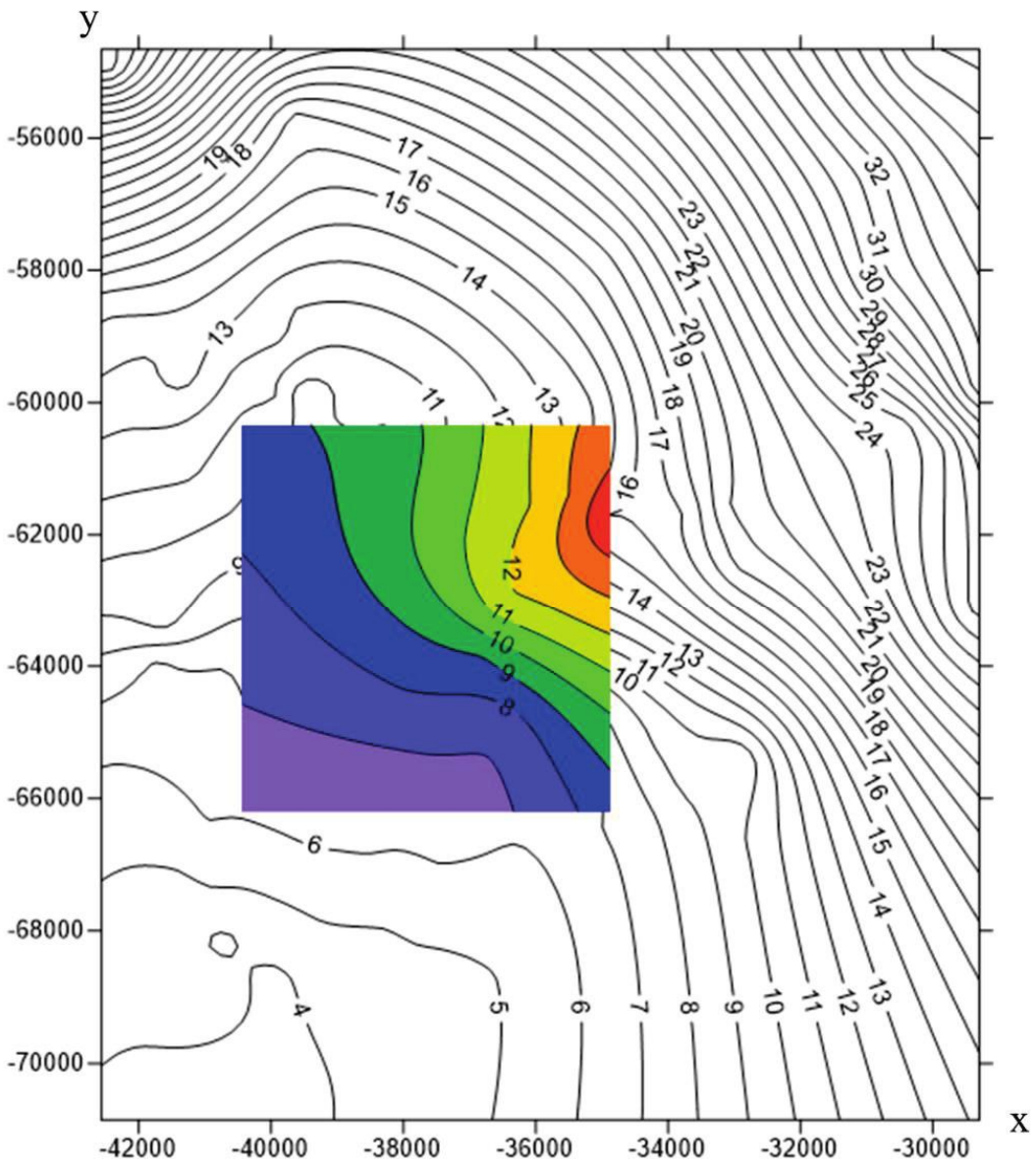

Figure 10. Groundwater level distribution on July 31-August 1, 2013 (rainbow color: average of groundwater level distribution by measured data of Ohtani et al., 2015)

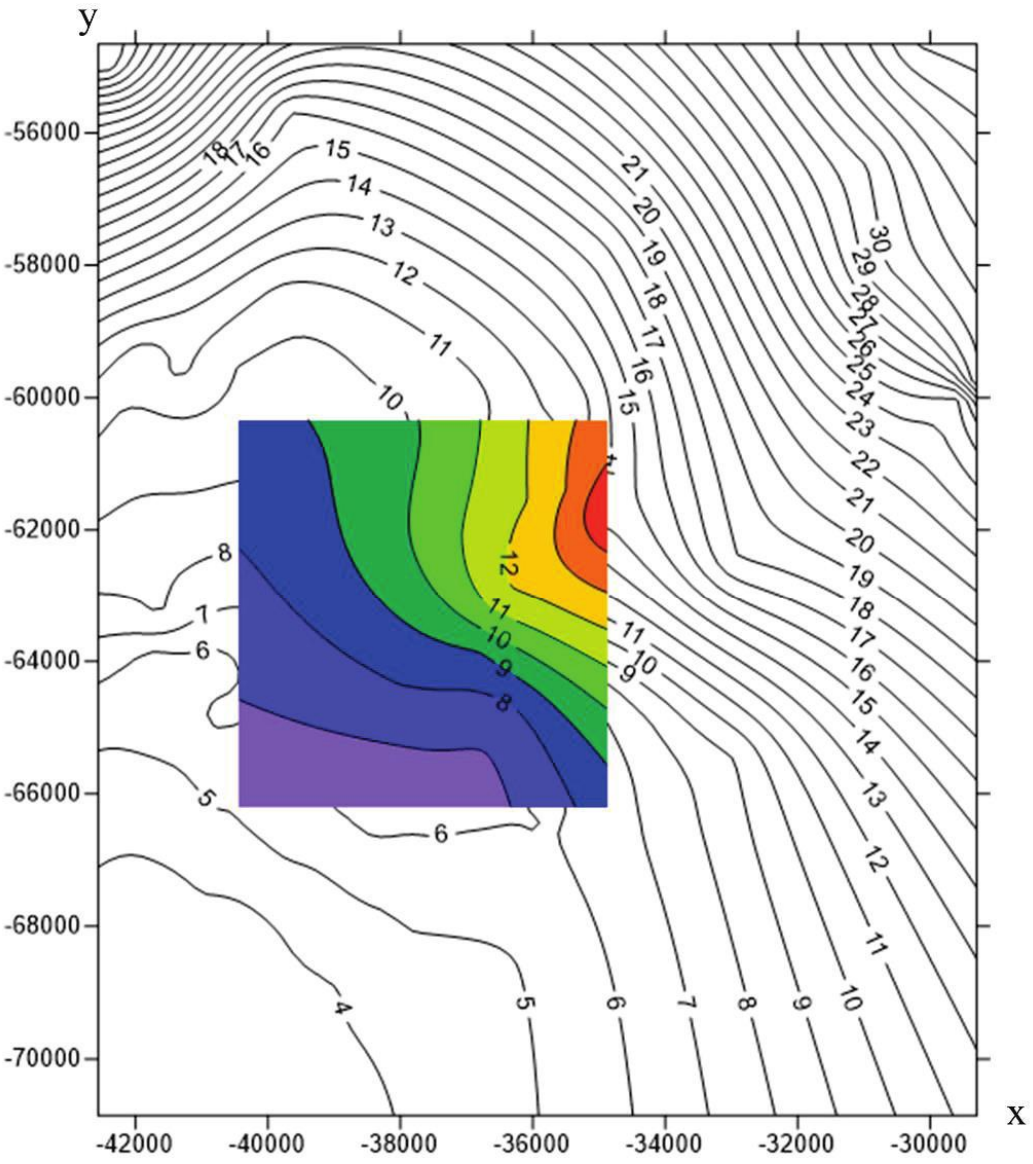

Figure 11. Groundwater level distribution on February 20-21, 2014 (rainbow color: average of groundwater level distribution by measured data of Ohtani et al., 2015)

2.3.1 Regional Simulation Model Settings

The model boundary was defined by the north-eastern mountainous area. There are no natural features in the south-east to south-west that could be utilized as model borders. Therefore, the model boundary is chosen by the hydraulic head contour line (Figure 12). The

horizontal dimensions of the model in east-west and north-south directions were 12 km and 12 km, respectively.

Polygon was created to define the model area boundaries. The outer model boundary is defined in the supermesh. The supermesh's polygons, lines, and points can subsequently be utilized to apply boundary conditions or material properties. After establishing the geometry and assigning the model's boundaries, the next step is to generate the mesh. A finite element mesh is used in the numerical simulation. The mesh was generated automatically by software. To obtain a finer mesh, we used the default triangle type element mesh with 6000 total element number. When compared to other mesh generation algorithms, triangle mesh is extremely fast and can handle complex polygon and point/line setups. The total number of mesh elements is 316,712, with geometry height 12,230 m and width 12,020 m. The finite element mesh was then converted to 2D geometry (Figure 13).

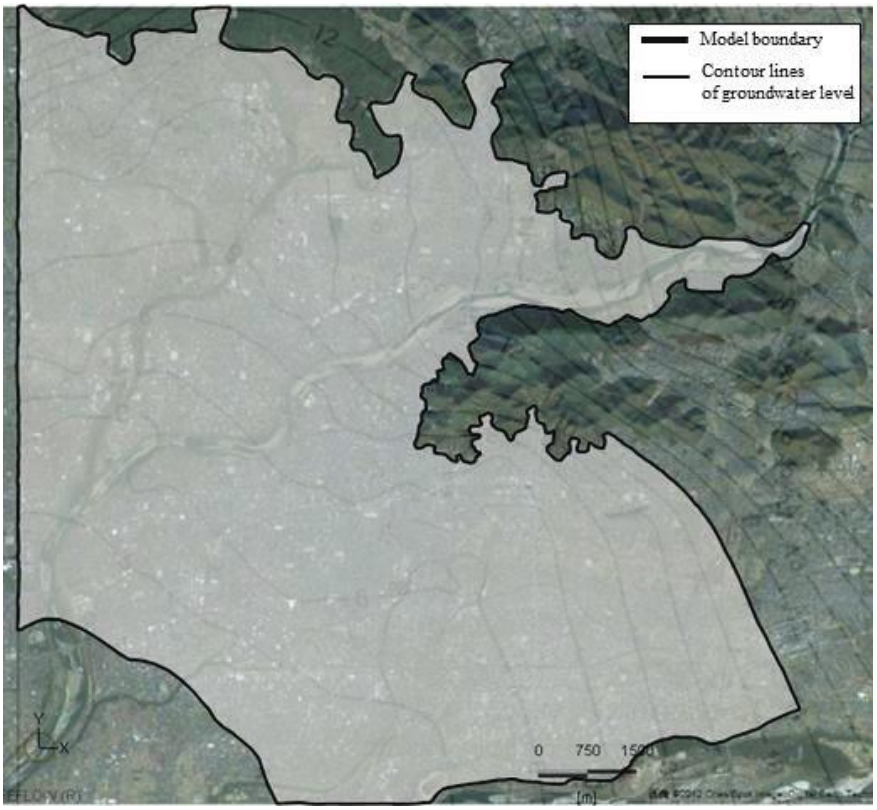

Figure 12 Outer polygon of the supermesh

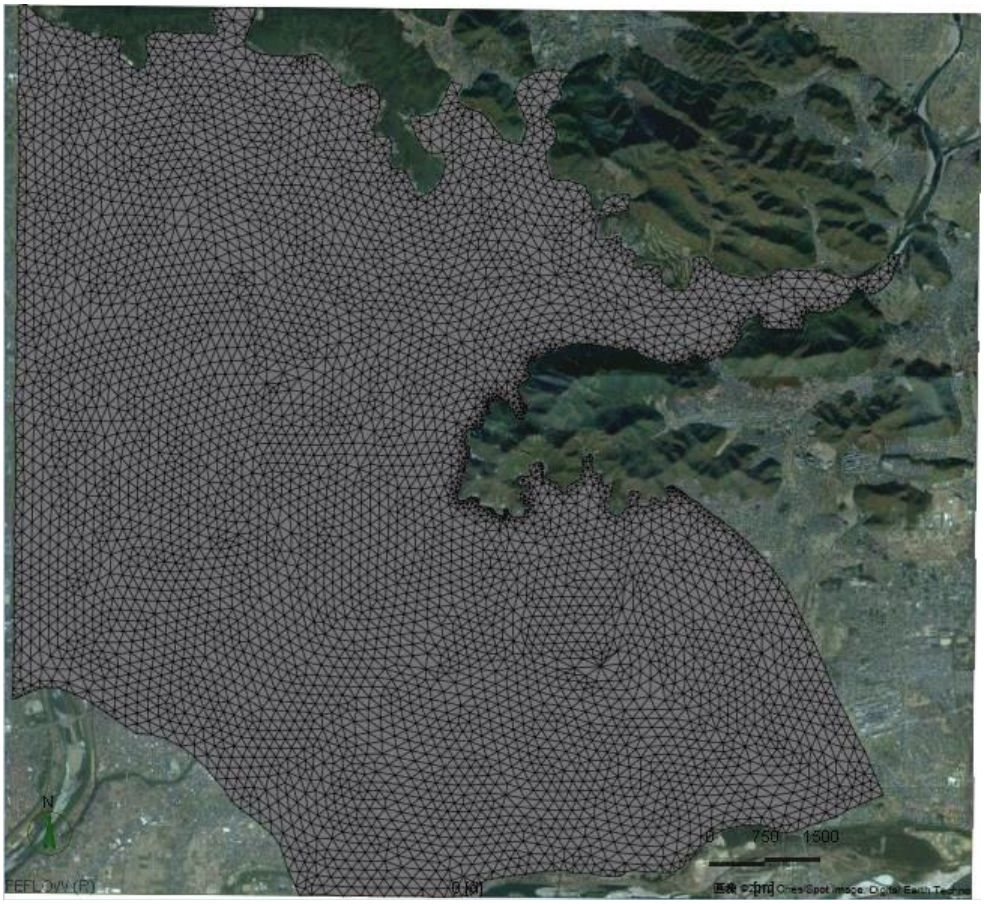

Figure 13. Finite-element mesh

We converted this 2D geometry into 3D geometry with multiple layers (Figure 14). The actual height of the layer from top to bottom was determined using geological column and profile data. The actual elevation of each geological layer top is calculated using map data interpolation. Geological data was compiled into an Excel spreadsheet (*.xlsx) with the following columns: X, Y, elevation, and slice. FEFLOW was used to connect the data files, which were then linked to a 3D layer setup. The layer model had 31 layers or 32 slices. There are 5,530 nodes per slice and 10,212 elements per layer. FEFLOW distinguishes between layers and slices in a 3D model. Layers are three-dimensional bodies that represent geological formations such as aquifers and aquitards. Slices are the interfaces between layers, as well as the top and bottom model boundaries.

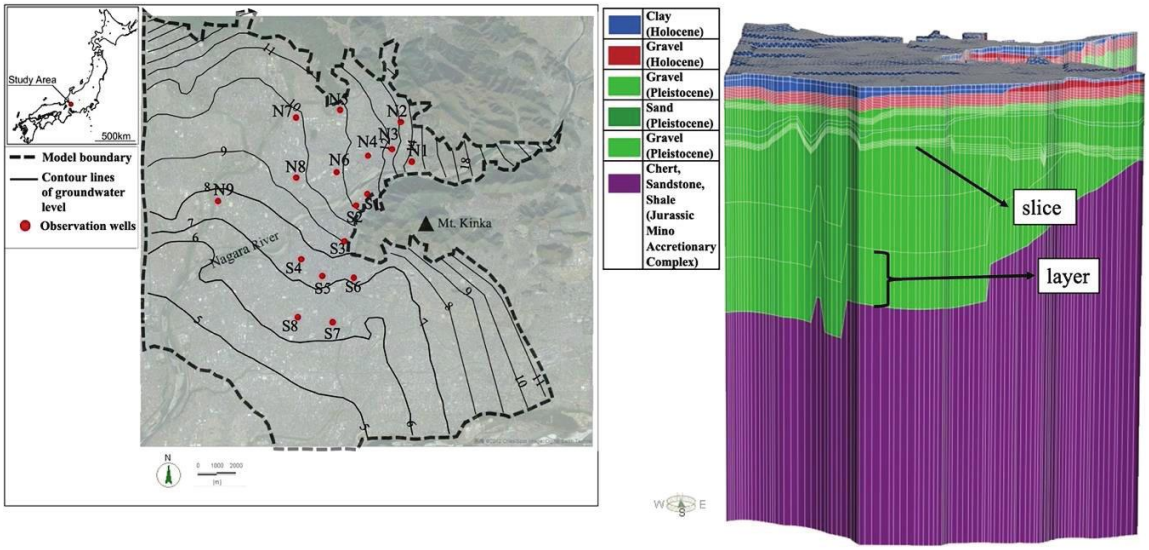

Figure 14. (Left) Model study area and measured hydraulic head distribution in winter (Gifu city). (Right) 3D geological model.

Layers 1-2 are clay (Holocene), layer 3-14 is gravel (Holocene), layer 15-20 is gravel (Pleistocene) in the first aquifer, layer 21-21 is sand (Pleistocene), layer 23-28 is gravel (Pleistocene) in the second aquifer, and layer 29-31 is Chert, Sandstone, Shale (Jurassic Mino Accretionary Complex) with a low permeability unit. Each layer was subdivided into additional slices to increase the quality of the numerical result of the first aquifer in line with groundwater flow given. The major aquifer gravel (Holocene) and gravel (Pleistocene) layers which unconsolidated sediments had set with 1 m distance depth (Table 1).

Boundary conditions must be established to enable flows into and out of the model. The groundwater level distribution in Gifu city was used to define the hydraulic-head boundary conditions. The hydraulic head was based on groundwater level measurement on 195 observation points at February 20-21, 2014. The groundwater level measurement data were contour mapped using SURFER software. Transient flow of groundwater flow due to groundwater level change may be important for groundwater temperature distribution in the study area. However, due to the limited data, we applied the groundwater level distribution on February 20-21, 2014 as the boundary condition of hydraulic head.

The value was set for all slice borders to the bottom of the gravel (Pleistocene) layer (Layer 28). On the northeast side, observation sites are limited, as you can see on Figure 16. After evaluation the results of fluid flow simulation, the groundwater level near the recharge area is far lower than measured. Therefore, the hydraulic-head boundary condition in this part was set according to the average of groundwater level at Nagara point and Akutami point (Figure 17) to increase the groundwater level results.

Table 1. Material properties for flow and heat transport

<table>
<tr><th rowspan="2">Layer</th><th rowspan="2">Geological layers</th><th rowspan="2">Thickness of each layer (m)</th><th>Flow</th><th colspan="2">Heat Transport</th></tr>
<tr><th>Conductivity (m/s)</th><th>Porosity (%)</th><th>Dispersivity (m)</th></tr>
<tr><td>1-2</td><td>Clay (Holocene)</td><td>1-4</td><td>$1x10^{-6}$</td><td rowspan="6">30</td><td rowspan="7">90 (longitudinal)
9 (transverse)</td></tr>
<tr><td>3-14</td><td>Gravel (Holocene)</td><td>1</td><td>$7x10^{-2}$</td></tr>
<tr><td>15-20</td><td>Gravel (Pleistocene)</td><td>1</td><td>$1x10^{-4}$</td></tr>
<tr><td>21</td><td>Sand (Pleistocene)</td><td>2-6</td><td>$5x10^{-5}$</td></tr>
<tr><td>22-27</td><td>Gravel (Pleistocene)</td><td>2-3</td><td rowspan="2">$1x10^{-4}$</td></tr>
<tr><td>28-30</td><td>Gravel (Pleistocene)</td><td><50</td></tr>
<tr><td>31</td><td>Chert, Sandstone, Shale (Jurassic Mino Accretionary Complex)</td><td><250</td><td>$1x10^{-8}$</td><td>10</td></tr>
</table>

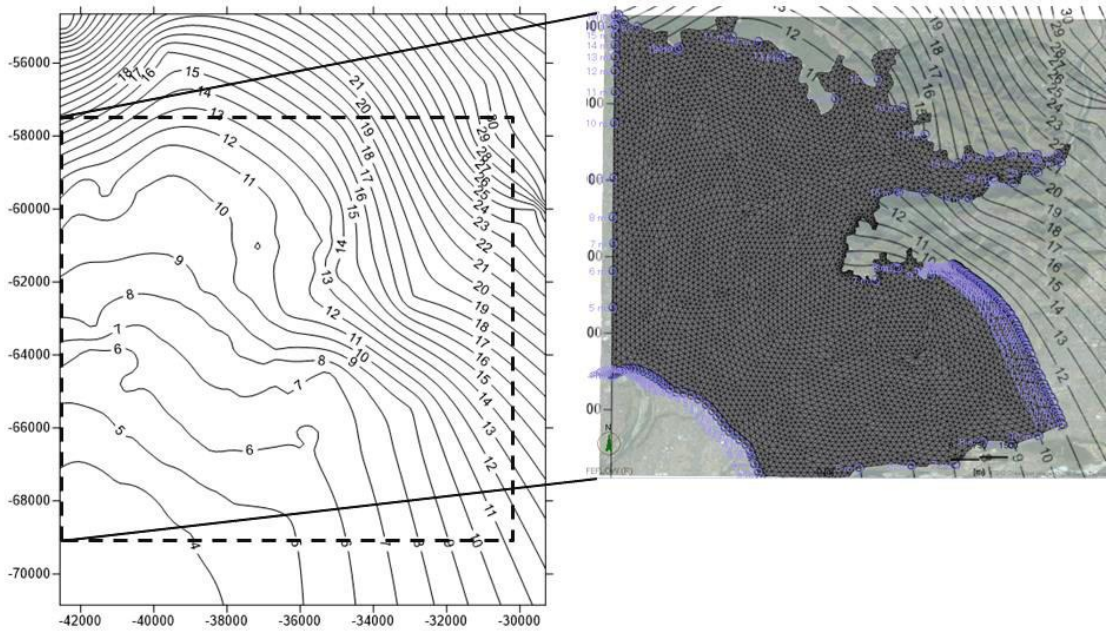

Figure 15. Fluid flux flow boundary condition

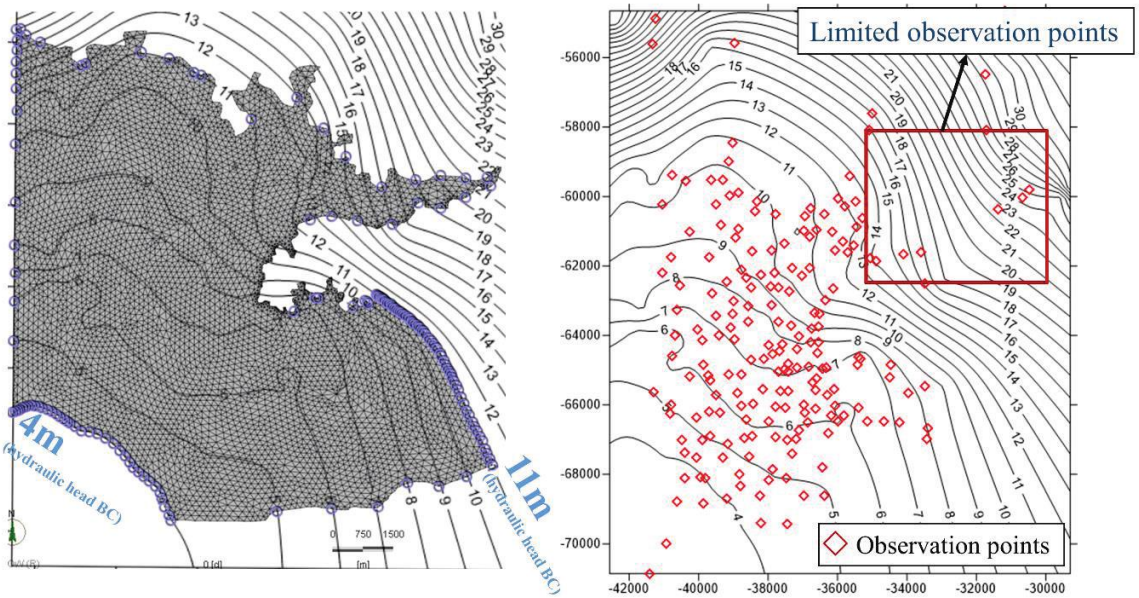

Figure 16. Fluid flux flow boundary condition limited observations

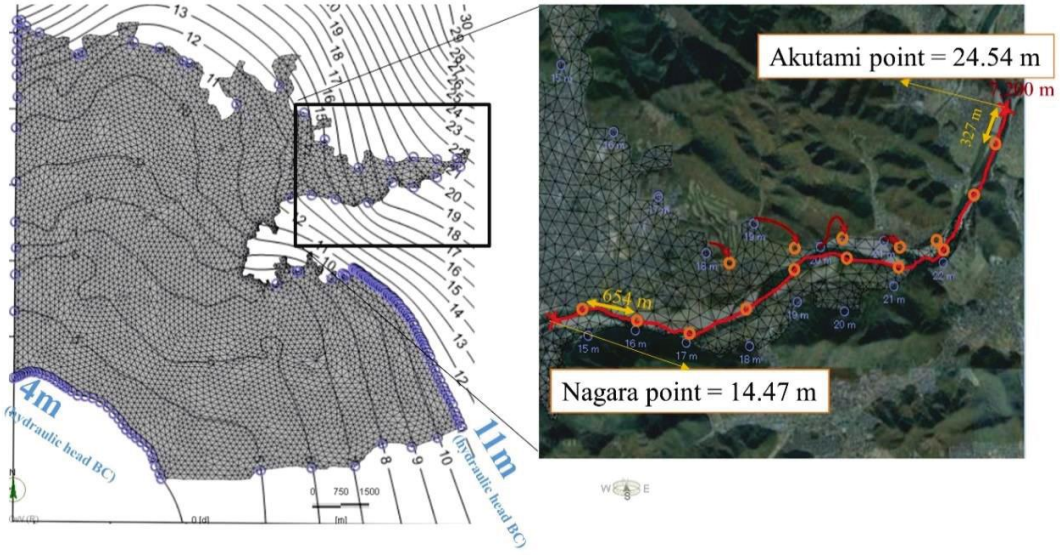

Figure 17. Groundwater level at Akutami point and Nagara point that used for hydraulic-head boundary condition on northeast side. Yellow circle: hydraulic-head boundary condition modified based on distance from Nagara point and Akutami point.

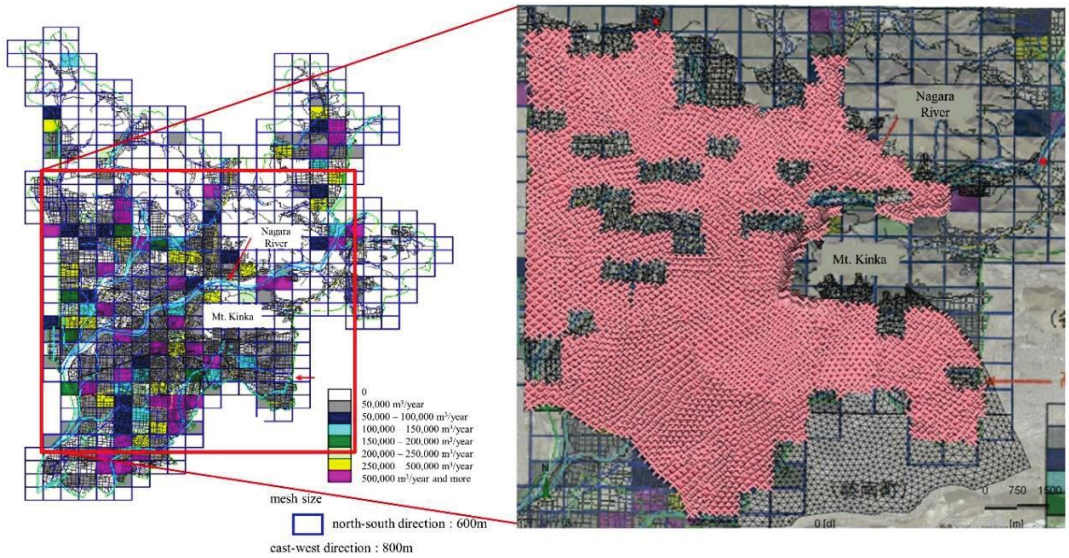

Figure 18. (Left) Reported groundwater extraction of Gifu City (Adapted from Gifu Prefecture, Gifu City, Teikoku Construction Consultant (2011), Report on feasibility study of geothermal heat pumps, 201p. (Right) Setting of pumping-rate boundary condition.

The fluid-flux boundary conditions were developed based on the pumping rate in the alluvial fan of the Nagara River using Teikoku Construction Company data (Figure 18). In the study area, groundwater is properly extracted. Groundwater extraction can have regional impacts on temperature trends because of changes in surface-subsurface water interactions. Pumping-rate boundary conditions were manually adjusted in the aquifer (slice 3-28) based on mesh size.

Groundwater recharges from the Nagara River in the alluvial fan. As shown in Figure 19, the recharge zone of the alluvial fan is assumed to be around the Nagara Bridge. This may be seen in observation wells monitored by Ohtani *et al.* (2015) . Temperature fluctuations decrease as one moves downstream of the groundwater flow. The upstream part of the groundwater flow was chosen as the location of the heat source. Time-varying boundary conditions are inserted from data on the time-series dialog based on temperature calculation data of the Nagara River. Top and bottom of the model are fixed by constant temperature boundaries. Surface temperature, which is primarily covered by asphalt, affects the top of the model. Bottom of the model is basement rock, treated as impermeable boundary and lateral sides are set as no flow boundaries. Initial temperatures of model were applied by average surface temperature (18 °C), subsurface temperature (16.3 °C), and bottom of the model (18 °C). Temperature of boundary conditions were set constant 18°C on surface and bottom of the model, then time series data of water temperature of the Nagara River were set at an recharge area in the upstream of the groundwater flow.

Parameters for subsurface flow and heat transport processes is shown on Table 1. Parameters are set in the 3D model according to reference data (Diersch, 2014; Lo Russo et al., 2014; Lo Russo and Civita, 2009; Meng et al., 2019; Ohtani et al., 2015). The values of volumetric heat capacity of fluid (4.2 MJ/m³/K), the volumetric heat capacity of solid (2.52 MJ/m³/K), the thermal conductivity of fluid (0.65 J/m/s/K), and thermal conductivity of solid (3 J/m/s/K) were given in the model layers. Dispersivity is one of effective factors of heat transport. The ratio of longitudinal to tranverse is assumed to be 10.

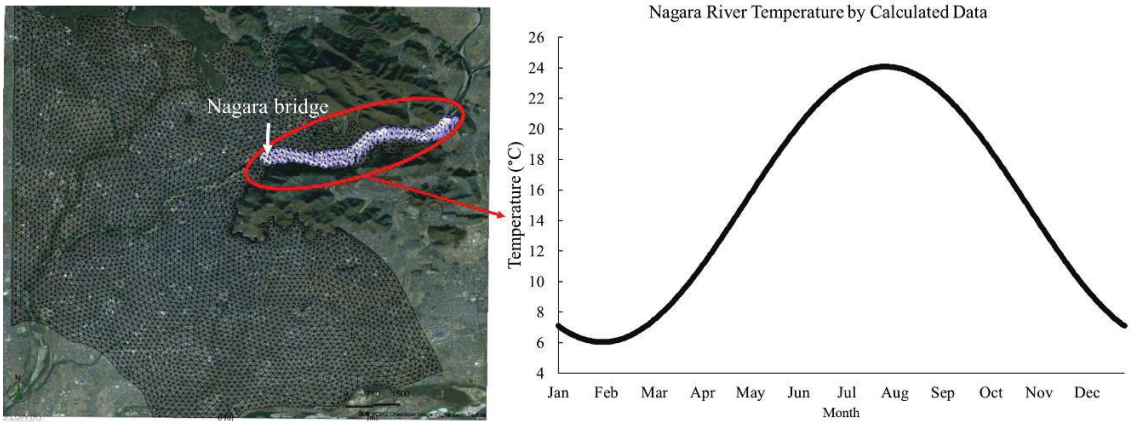

Figure 19. (Left) The area setting the Temperature Boundary Condition as a recharge zone, (Right) Temperature change of the recharge zone.

The simulation results were calibrated against measured data from observation points. Observation points were added in the model based on the location of observation wells. Measurements of groundwater level and groundwater temperature distribution were used to confirm the simulation results (Figure 7-8). Ohtani et al. (2015) monitored these observation points at monthly intervals across the Gifu city region from May 2013 to May 2014.

If there is no agreement on that validation, some parameters will be determined by trial and error. Calibration is required for some variables using sensitivity analysis due to their higher degrees of uncertainty. If the validation findings were agreed, the regional model parameter values were used to build the local simulation model.

2.3.2 Sensitivity Analysis

Sensitivity analysis is carried out in order to determine the right parameters for the regional simulation model. This was conducted due to limited data on geological and hydrological conditions in the study area. Parameters that greatly affect the model simulation results are dispersivity, initial temperature, hydraulic conductivity, and pumping rate according to sensitivity analysis.

Dispersivity come from chart of measured longitudinal dispersivities in relation to the spatial scale from FEFLOW 6.1 Training Manual book, showed on Figure 20. Dispersion

occurs due to differences in transport velocities caused by matrix variations (microdispersivity) and by geological inhomogeneities of larger spatial scales (macrodispersivity). Dispersion is usually considered by applying the linear Bear-Scheidegger dispersivity law, which distinguishes between a dispersivity parameter in flow direction (longitudinal dispersivity) and a dispersivity parameter perpendicular to the flow direction (transverse dispersivity). The longitudinal dispersivity depends on the length scale of the phenomenon. It is applied according to reasonable value on the calibration. After trying various values of dispersivity, the ideal values for simulation model are longitunal 90 m and transverse 9m. As can be seen from the sensitivity analysis of dispersivity in Table 2 for settings and Table 3 for the results.

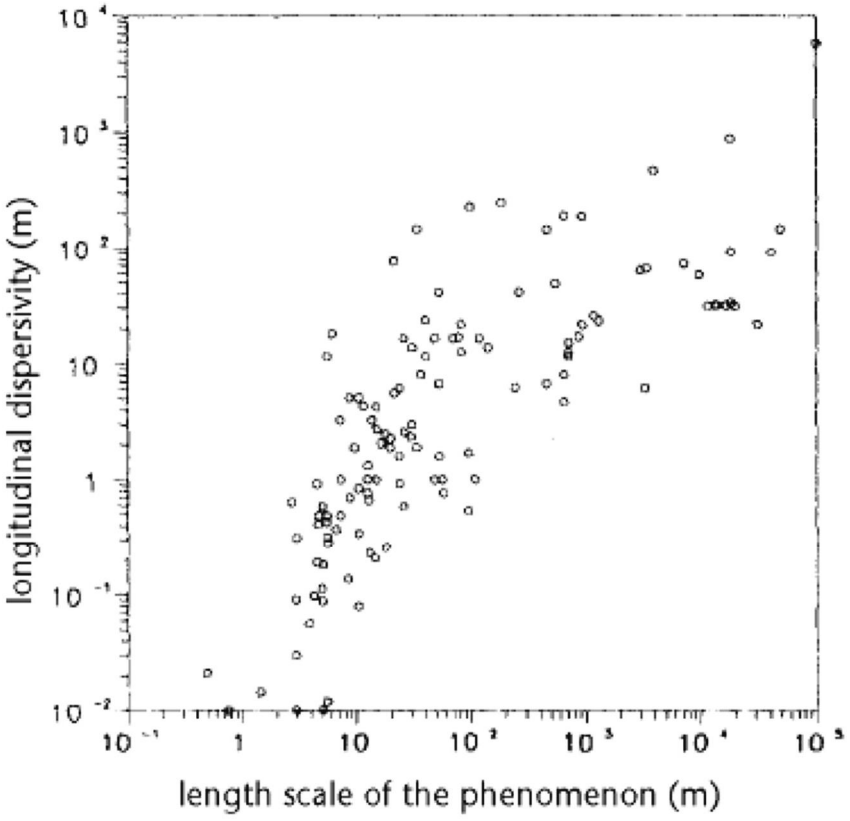

Figure 20. Longitudinal dispersivity vs scale of phenomenon (source: FEFLOW 6.1 Training Manual, DHI-WASY GmbH, Groundwater Modeling Centre, FEFLOW Services, 2013)

Table 2. The sensitivity analysis of dispersivity (settings)

Modification	Case	Geological Layer	Hydraulic Conductivity (m/s)	Initial Temperature (°C)	Porosity (%)	Dispersivity (m)
Dispersivity	Case 1	Clay (Holocene)	1.0×10^{-6}	18	30	Longitudinal = 45 m Transverse = 4.5 m
		Gravel (Holocene)	7.0×10^{-2}	16.3		
		Gravel (Pleistocene)	1.0×10^{-4}			
		Sand (Pleistocene)	5.0×10^{-5}			
		Gravel (Pleistocene)	1.0×10^{-4}			
		Chert, Sandstone, Shale (Jurassic Mino Accretionary Complex)	1.0×10^{-8}	18	10	
	Case 2	Clay (Holocene)	1.0×10^{-6}	18	30	Longitudinal = 55 m Transverse = 5.5 m
		Gravel (Holocene)	7.0×10^{-2}	16.3		
		Gravel (Pleistocene)	1.0×10^{-4}			
		Sand (Pleistocene)	5.0×10^{-5}			
		Gravel (Pleistocene)	1.0×10^{-4}			

		Chert, Sandstone, Shale (Jurassic Mino Accretionary Complex)	$1.0x10^{-8}$	18	10	
	Case 3	Clay (Holocene)	$1.0x10^{-6}$	18	30	Longitudinal = 90 m Transverse = 9 m
		Gravel (Holocene)	$7.0x10^{-2}$	16.3		
		Gravel (Pleistocene)	$1.0x10^{-4}$			
		Sand (Pleistocene)	$5.0x10^{-5}$			
		Gravel (Pleistocene)	$1.0x10^{-4}$			
		Chert, Sandstone, Shale (Jurassic Mino Accretionary Complex)	$1.0x10^{-8}$	18	10	
	Case 4	Clay (Holocene)	$1.0x10^{-6}$	18	30	Longitudinal = 100 m Transverse = 10 m
		Gravel (Holocene)	$7.0x10^{-2}$	16.3		
		Gravel (Pleistocene)	$1.0x10^{-4}$			
		Sand (Pleistocene)	$5.0x10^{-5}$			

		Gravel (Pleistocene)	$1.0x10^{-4}$			
		Chert, Sandstone, Shale (Jurassic Mino Accretionary Complex)	$1.0x10^{-8}$	18	10	
	Case 5	Clay (Holocene)	$1.0x10^{-6}$	18	30	Longitudinal = 900 m Transverse = 90 m
		Gravel (Holocene)	$7.0x10^{-2}$	16.3		
		Gravel (Pleistocene)	$1.0x10^{-4}$			
		Sand (Pleistocene)	$5.0x10^{-5}$			
		Gravel (Pleistocene)	$1.0x10^{-4}$			
		Chert, Sandstone, Shale (Jurassic Mino Accretionary Complex)	$1.0x10^{-8}$	18	10	

Table 3. The sensitivity analysis of dispersivity (results)

Modification	Case	Results
Dispersivity	1	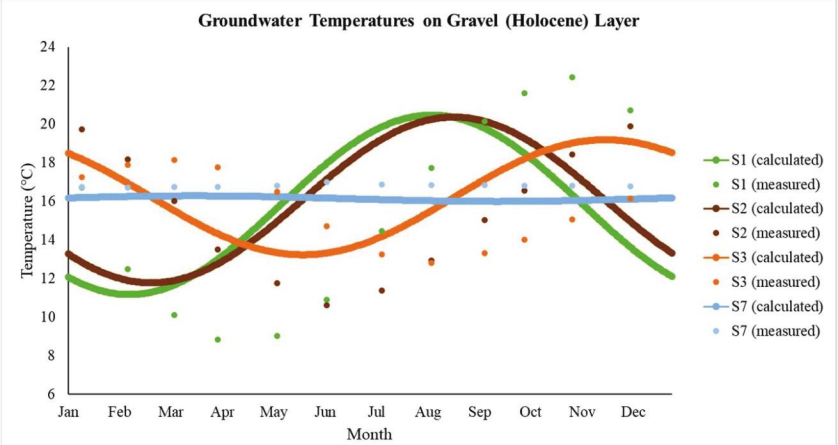
	2	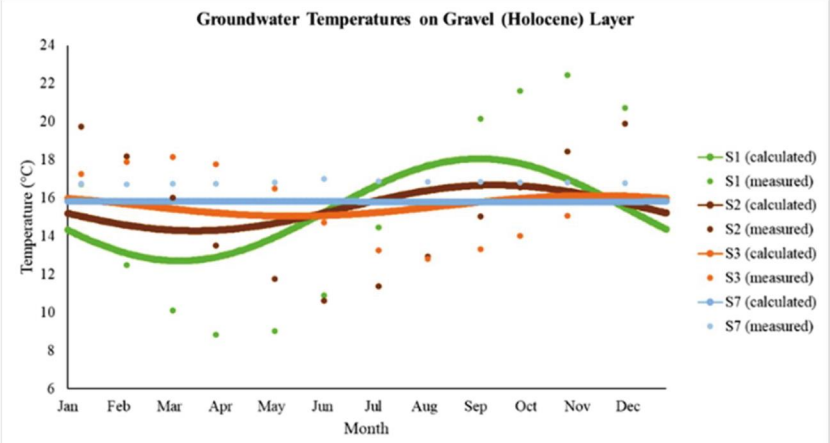
	3	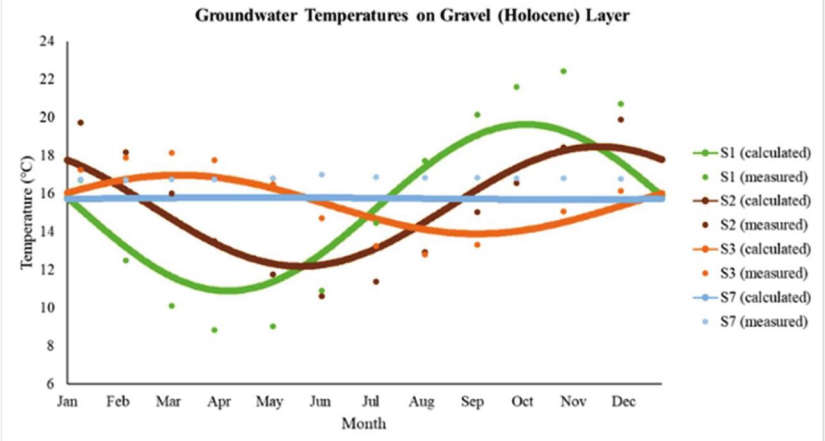

	4	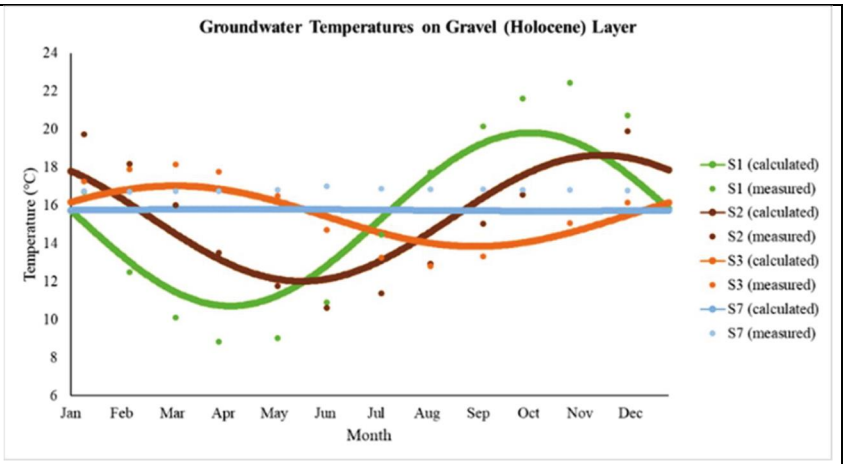
	5	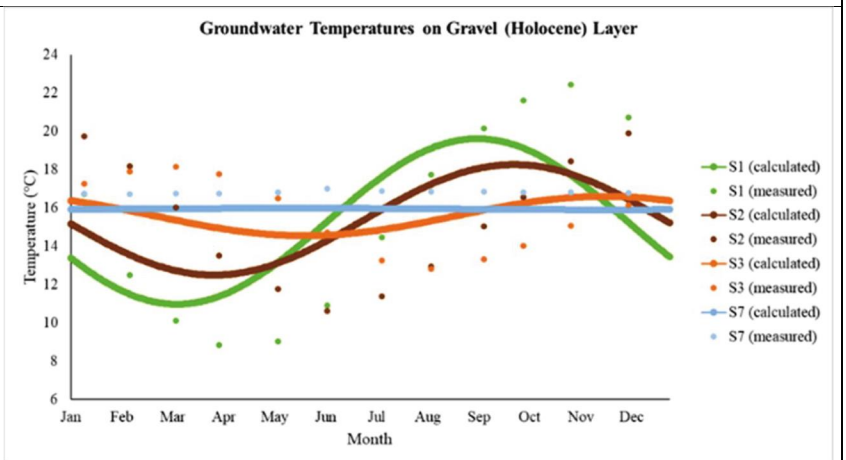

At ground surface, ground temperatures are affected by seasonal atmospheric temperature changes. Surface temperature, which is mostly covered by asphalt, thus affecting surface temperature. Therefore, it is set constant temperature for surface temperature. The initial temperature value affects the change in groundwater temperature in the Holocene gravel layer, as can be seen in the sensitivity analysis of the initial temperature (Table 4 for settings and Table 5 for results). Initial temperatures of model were applied by average surface temperature (22.5 °C), subsurface temperature (16.3 °C), and bottom of the model (18 °C).

Table 4. The sensitivity analysis of the initial temperature (settings)

Modification	Case	Geological Layer	Hydraulic Conductivity (m/s)	Initial Temperature (°C)	Porosity (%)	Dispersivity (m)
Initial Temperature	Case 1	Clay (Holocene)	$1.0x10^{-2}$	22.5	30	Longitudinal = 90 m Transverse = 9 m
		Gravel (Holocene)	$1.5x10^{-1}$	16.3		
		Gravel (Pleistocene)	$2.0x10^{-3}$			
		Sand (Pleistocene)	$5.0x10^{-5}$			
		Gravel (Pleistocene)	$1.0x10^{-3}$			
		Chert, Sandstone, Shale (Jurassic Mino Accretionary Complex)	$1.0x10^{-8}$	18	10	
	Case 2	Clay (Holocene)	$1.0x10^{-2}$	18	30	Longitudinal = 90 m Transverse = 9 m
		Gravel (Holocene)	$1.5x10^{-1}$	16.3		
		Gravel (Pleistocene)	$2.0x10^{-3}$			
		Sand (Pleistocene)	$5.0x10^{-5}$			
		Gravel (Pleistocene)	$1.0x10^{-3}$			
		Chert, Sandstone,	$1.0x10^{-8}$	18	10	

		Shale (Jurassic Mino Accretionary Complex)				

Table 5. The sensitivity analysis of the initial temperature (results)

Modification	Case	Results
Initial Temperature	1	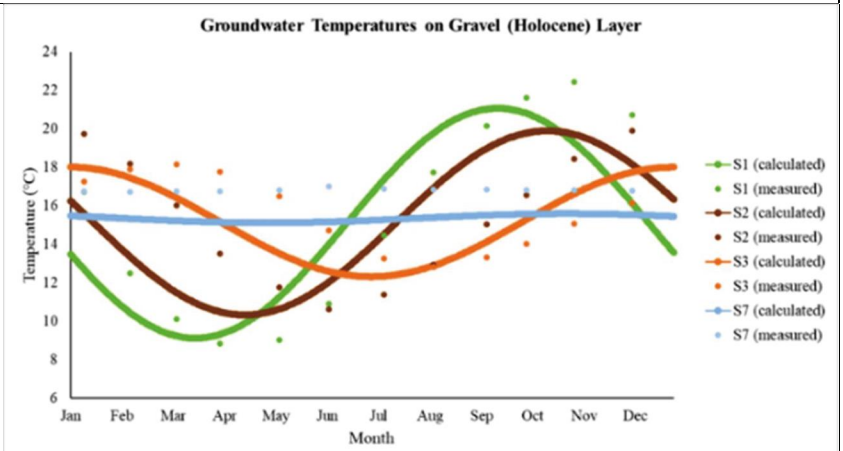
	2	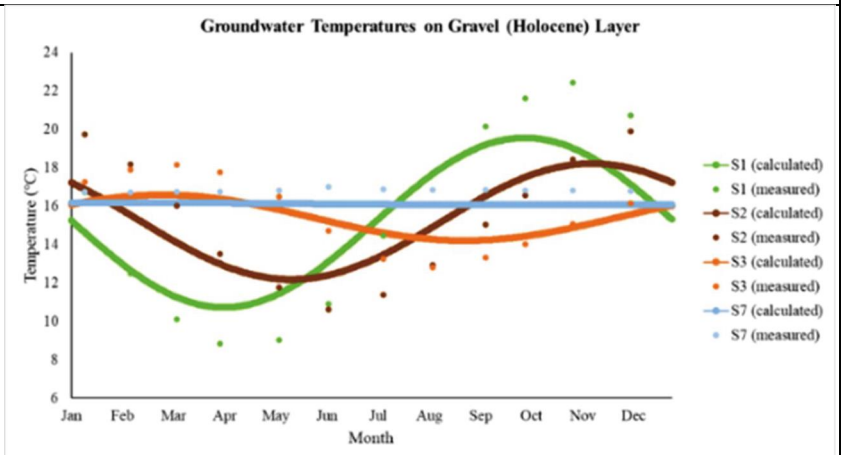

Hydraulic conductivity is very important for waterflow in the formations. In this study, the assumed hydraulic conductivity of each formation type for the different layers were given. Among the various modified parameters, hydraulic conductivity is the most influenced value for the groundwater temperature distribution. This can be seen in the sensitivity analysis of the hydraulic conductivity in Table 6 (settings) and Table 7 (results). Because the groundwater flow in the Holocene gravel is very fast, after trial, the value of 0.07 m/s is appropriate, as seen in the sensitivity analysis of hydraulic conductivity. To increase the maximum groundwater temperature value, we will increase the pumping rate and initial temperature subsequently. The clay (Holocene) and gravel (Pleistocene) values are set very small compared to the gravel (Holocene) value. This is due to the fact that groundwater flow occurs mainly in the first aquifer, as we can see from the groundwater temperature measurement data in S3 from the following Figure 6.

Table 6. The sensitivity analysis of the hydraulic conductivity (settings)

Modification	**Case**	**Geological Layer**	**Hydraulic Conductivity (m/s)**	**Initial Temperature (ºC)**	**Porosity (%)**	**Dispersivity (m)**
Hydraulic conductivity	Case 1	Clay (Holocene)	$1.0x10^{-2}$	18	30	Longitudinal = 90 m Transverse = 9 m
		Gravel (Holocene)	$1.5x10^{-1}$	16.4		
		Gravel (Pleistocene)	$2.0x10^{-3}$			
		Sand (Pleistocene)	$5.0x10^{-5}$			
		Gravel (Pleistocene)	$1.0x10^{-3}$			
		Chert, Sandstone, Shale (Jurassic	$1.0x10^{-8}$	18	10	

		Mino Accretionary Complex)				
	Case 2	Clay (Holocene)	$1.0x10^{-6}$	22.5	30	Longitudinal = 90 m Transverse = 9 m
		Gravel (Holocene)	$9.0x10^{-2}$	16.3		
		Gravel (Pleistocene)	$1.0x10^{-4}$			
		Sand (Pleistocene)	$5.0x10^{-5}$			
		Gravel (Pleistocene)	$1.0x10^{-4}$			
		Chert, Sandstone, Shale (Jurassic Mino Accretionary Complex)	$1.0x10^{-8}$	18	10	
	Case 3	Clay (Holocene)	$1.0x10^{-6}$	22.5	30	Longitudinal = 90 m Transverse = 9 m
		Gravel (Holocene)	$7.0x10^{-2}$	16.3		
		Gravel (Pleistocene)	$1.0x10^{-4}$			
		Sand (Pleistocene)	$5.0x10^{-5}$			
		Gravel (Pleistocene)	$1.0x10^{-4}$			
		Chert, Sandstone, Shale	$1.0x10^{-8}$	18	10	

		(Jurassic Mino Accretionary Complex)				
	Case 4	Clay (Holocene)	$1.0x10^{-6}$	22.5	30	Longitudinal = 90 m Transverse = 9 m
		Gravel (Holocene)	$7.0x10^{-2}$	16.3		
		Gravel (Pleistocene)	$1.0x10^{-3}$			
		Sand (Pleistocene)	$5.0x10^{-5}$			
		Gravel (Pleistocene)	$1.0x10^{-4}$			
		Chert, Sandstone, Shale (Jurassic Mino Accretionary Complex)	$1.0x10^{-8}$	18	10	
	Case 5	Clay (Holocene)	$1.0x10^{-6}$	22.5	30	Longitudinal = 90 m Transverse = 9 m
		Gravel (Holocene)	$5.0x10^{-2}$	16.3		
		Gravel (Pleistocene)	$1.0x10^{-4}$			
		Sand (Pleistocene)	$5.0x10^{-5}$			
		Gravel (Pleistocene)	$1.0x10^{-4}$			
		Chert, Sandstone,	$1.0x10^{-8}$	18	10	

		Shale (Jurassic Mino Accretionary Complex)				

Table 7. The sensitivity analysis of the hydraulic conductivity (results)

Modification	Case	Results
Hydraulic conductivity	1	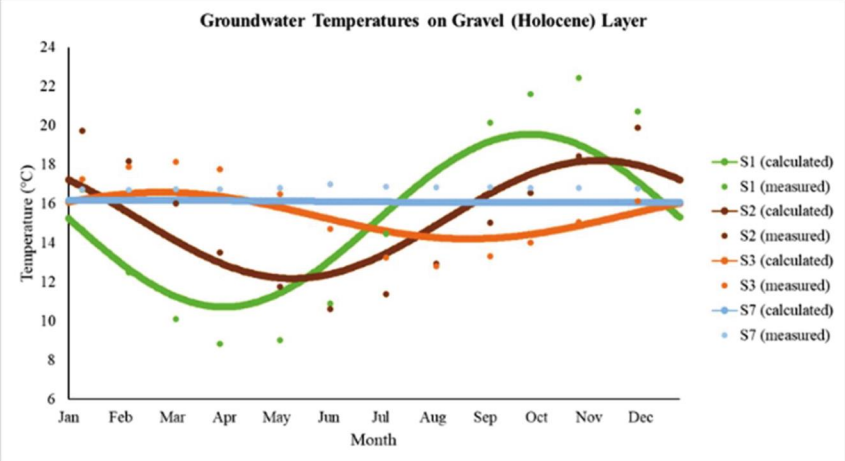
	2	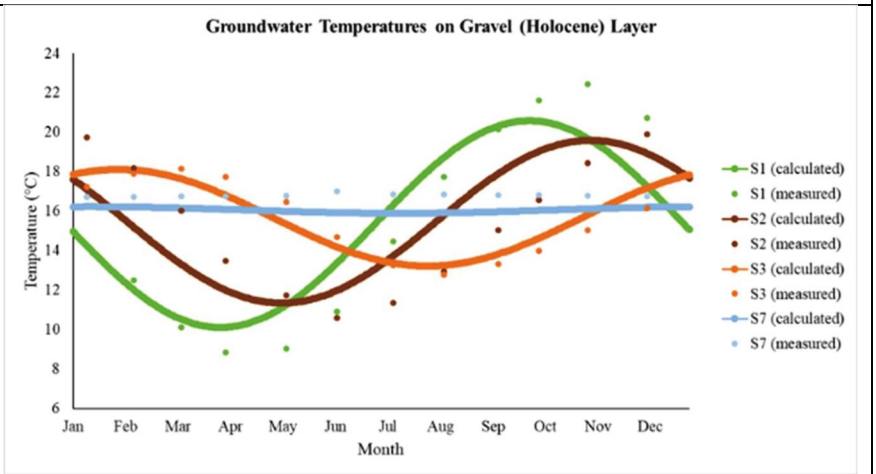

	3	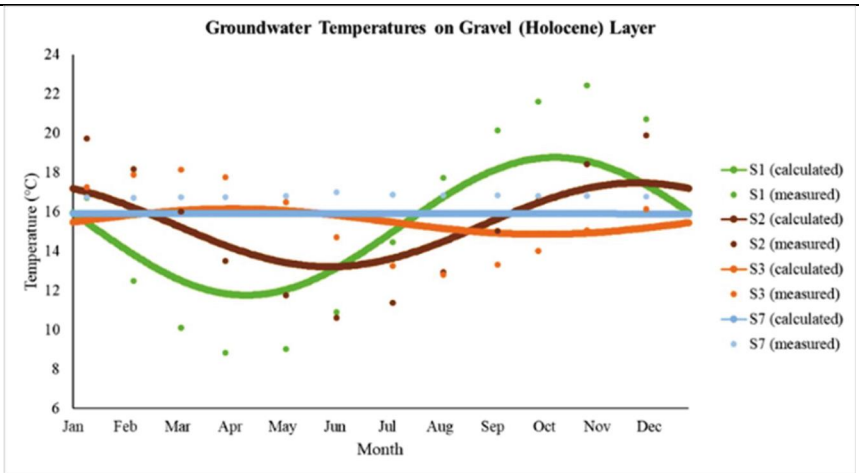 Groundwater Temperatures on Gravel (Holocene) Layer Temperature (°C) Month Jan Feb Mar Apr May Jun Jul Aug Sep Oct Nov Dec 6 8 10 12 14 16 18 20 22 24 S1 (calculated) S1 (measured) S2 (calculated) S2 (measured) S3 (calculated) S3 (measured) S7 (calculated) S7 (measured)
	4	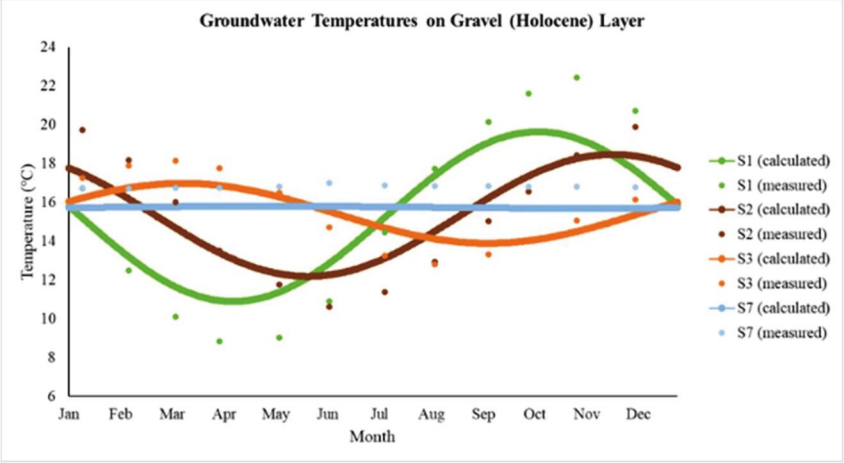 Groundwater Temperatures on Gravel (Holocene) Layer Temperature (°C) Month Jan Feb Mar Apr May Jun Jul Aug Sep Oct Nov Dec 6 8 10 12 14 16 18 20 22 24 S1 (calculated) S1 (measured) S2 (calculated) S2 (measured) S3 (calculated) S3 (measured) S7 (calculated) S7 (measured)
	5	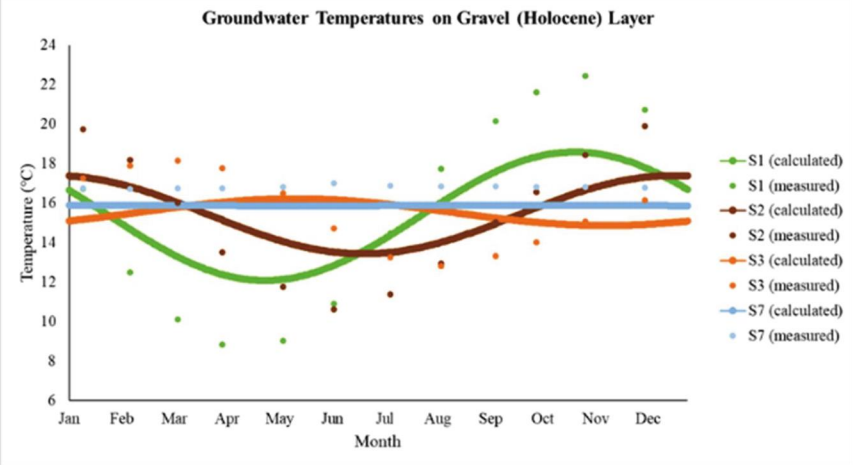 Groundwater Temperatures on Gravel (Holocene) Layer Temperature (°C) Month Jan Feb Mar Apr May Jun Jul Aug Sep Oct Nov Dec 6 8 10 12 14 16 18 20 22 24 S1 (calculated) S1 (measured) S2 (calculated) S2 (measured) S3 (calculated) S3 (measured) S7 (calculated) S7 (measured)

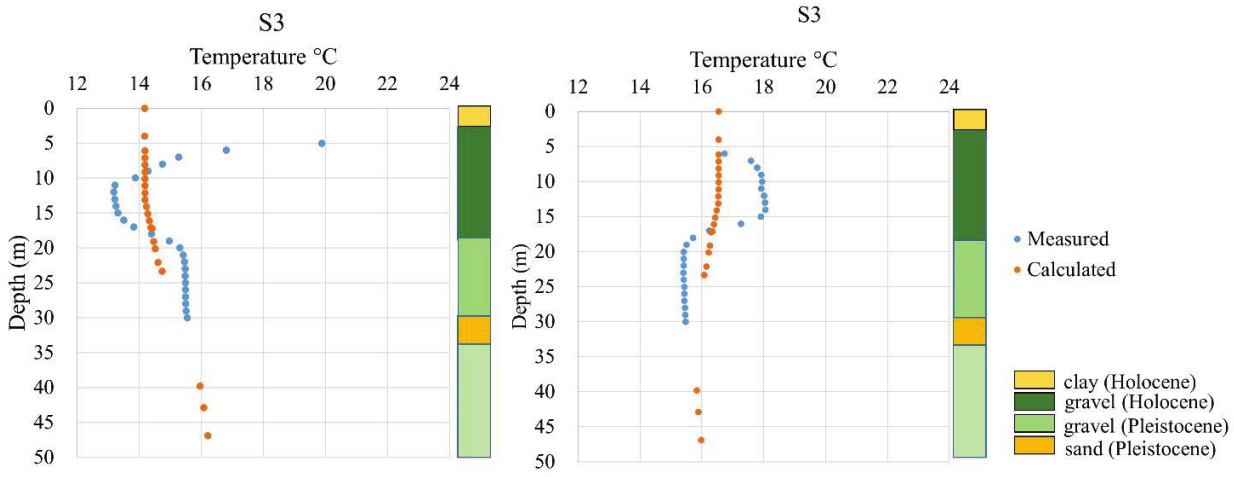

Figure 21. Temperature profile at S3 observation point with hydraulic conductivity values of gravel (Holocene) 1.5 x 10^{-1} m/s and gravel (Pleistocene) 2 x 10^{-3} m/s

Figure 21 is an example of temperature profile at S3 observation point with setting high conductivity value of the gravel (Holocene) layer (1.5x10^{-1}m/s) and gravel (Pleistocene) layer (2x10^{-3} m/s). Groundwater temperature change is not concentrated in the gravel (Holocene) layer only, but also distributing to gravel (Pleistocene) layer. Therefore, the value of hydraulic conductivity is changed to be smaller in clay (Holocene) and sand and gravel (Pleistocene). As a result, groundwater temperatures can be concentrated in gravel layers with smaller Pleistocene gravel values 1x10^{-4} m/s, and the values in Holocene gravel layers are relatively smaller (7x10^{-2} m/s) than 1.5x10^{-1} m/s as can be seen in Figure 22.

Table 8 describes the sensitivity analysis between hydraulic conductivity and dispersivity. From this table we can see the interrelationship between hydraulic conductivity as groundwater flow and dispersivity as heat transport. From the several trials above, the value of hydraulic conductivity of Holocene gravel layers 7x10^{-2} m/s and dispersivity of longitudinal 90 m, tranverse 9 m is the most suitable to be applied in the simulation model.

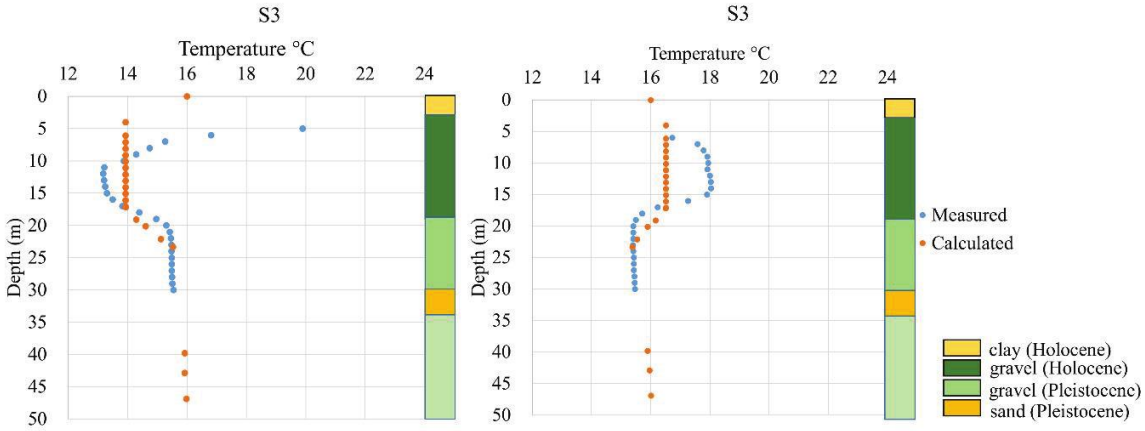

Figure 22. Temperature profile at S3 observation point with hydraulic conductivity values of gravel (Holocene) $7x10^{-2}$m/s and gravel (Pleistocene) $1x10^{-4}$ m/s

Table 8. The sensitivity analysis between hydraulic conductivity and dispersivity

*Measured value (S3) = 18.14 °C (max), 12.80 °C (min), 03/06 (maximum point on date), 0.55 year (phase difference)

Conductivity / Dispersivity	**1.5×10^{-1} m/s**	**1.0×10^{-1} m/s**	**9.0×10^{-2} m/s**	**7.0×10^{-2} m/s**	**5.0×10^{-2} m/s**
Longitudinal = 900 m Transverse = 90 m				(S3) : 16.60 °C (max), 14.55°C (min) Max point: 11/19 (date) Phase difference: 0.31 year	
Longitudinal = 100 m Transverse = 10 m				(S3) : 17.02 °C (max), 13.84°C (min) Max point: 03/03 (date)	

				Phase difference: 0.60 year	
Longitudinal = 90 m Transverse = 9 m	(S3) : 19.72 °C (max), 10.80°C (min) Max point: 11/20 (date) Phase difference: 0.32 year	(S3) : 18.19 °C (max), 12.50°C (min) Max point: 01/09 (date) Phase difference: 0.45 year	(S3) : 17.80 °C (max), 12.93°C (min) Max point: 01/25 (date) Phase difference: 0.50 year	(S3) : 16.98 °C (max), 13.89°C (min) Max point: 03/07 (date) Phase difference: 0.61 year	(S3) : 16.22 °C (max), 14.86°C (min) Max point: 05/11 (date) Phase difference: 0.79 year
Longitudinal = 70 m Transverse = 7 m				(S3) : 16.49 °C (max), 14.43°C (min) Max point: 03/17 (date) Phase difference: 0.64 year	
Longitudinal = 55 m Transverse = 5.5 m				(S3) : 16.12 °C (max), 15.05°C (min) Max point: 11/14 (date) Phase difference: 0.30 year	
Longitudinal = 45 m Transverse = 4.5 m				(S3) : 19.20 °C (max), 13.23°C (min) Max point: 11/18 (date)	

				Phase difference: 0.31 year	

Changes in surface-subsurface water interactions may have a regional influence on temperature trends due to groundwater extraction. This can be proven by the sensitivity analysis of the pumping rate shown in Table 9 for settings and Table 10 for results. The groundwater temperature in the Holocene gravel layer increases compared to without the application of the pumping rate. Pumping rate in the alluvial fan of the Nagara River based on Teikoku Construction Company data as shown in Figure 18. The application of several folds in Table 6 is aimed to find out the impact if the pumping rate value is adjusted in the model simulation.

Table 9. The sensitivity analysis of the pumping rate (settings)

Modification	**Case**	**Geological Layer**	**Hydraulic Conductivity (m/s)**	**Initial Temperature (ºC)**	**Porosity (%)**	**Dispersivity (m)**
Pumping rate	Case 1 (no pumping)	Clay (Holocene)	$5.0x10^{-3}$	18.2	30	Longitudinal = 90 m Transverse = 9 m
		Gravel (Holocene)	$1.5x10^{-1}$	17.4		
		Gravel (Pleistocene)	$2.0x10^{-3}$			
		Sand (Pleistocene)	$5.0x10^{-5}$			
		Gravel (Pleistocene)	$1.0x10^{-3}$			
		Chert, Sandstone, Shale (Jurassic Mino	$1.0x10^{-7}$	18	10	

		Accretionary Complex)				
	Case 2 (pumping applied)	Clay (Holocene)	$5.0x10^{-3}$	18.2	30	Longitudinal = 90 m Transverse = 9 m
		Gravel (Holocene)	$1.5x10^{-1}$	17.4		
		Gravel (Pleistocene)	$2.0x10^{-3}$			
		Sand (Pleistocene)	$5.0x10^{-5}$			
		Gravel (Pleistocene)	$1.0x10^{-3}$			
		Chert, Sandstone, Shale (Jurassic Mino Accretionary Complex)	$1.0x10^{-7}$	18	10	
	Case 3 (10 multiples)	Clay (Holocene)	$5.0x10^{-3}$	18.2	30	Longitudinal = 90 m Transverse = 9 m
		Gravel (Holocene)	$1.5x10^{-1}$	17.4		
		Gravel (Pleistocene)	$2.0x10^{-3}$			
		Sand (Pleistocene)	$5.0x10^{-5}$			
		Gravel (Pleistocene)	$1.0x10^{-3}$			
		Chert, Sandstone, Shale (Jurassic	$1.0x10^{-7}$	18	10	

		Mino Accretionary Complex)				
	Case 4 (100 multiples)	Clay (Holocene)	$5.0x10^{-3}$	18.2	30	Longitudinal = 90 m Transverse = 9 m
		Gravel (Holocene)	$1.5x10^{-1}$	17.4		
		Gravel (Pleistocene)	$2.0x10^{-3}$			
		Sand (Pleistocene)	$5.0x10^{-5}$			
		Gravel (Pleistocene)	$1.0x10^{-3}$			
		Chert, Sandstone, Shale (Jurassic Mino Accretionary Complex)	$1.0x10^{-7}$	18	10	

Table 10. The sensitivity analysis of the pumping rate (results)

Modification	Case	Results
Pumping rate	1	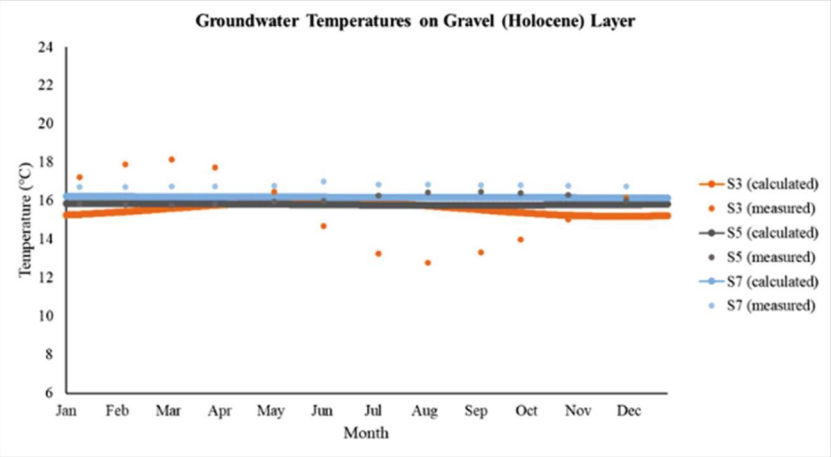
	2	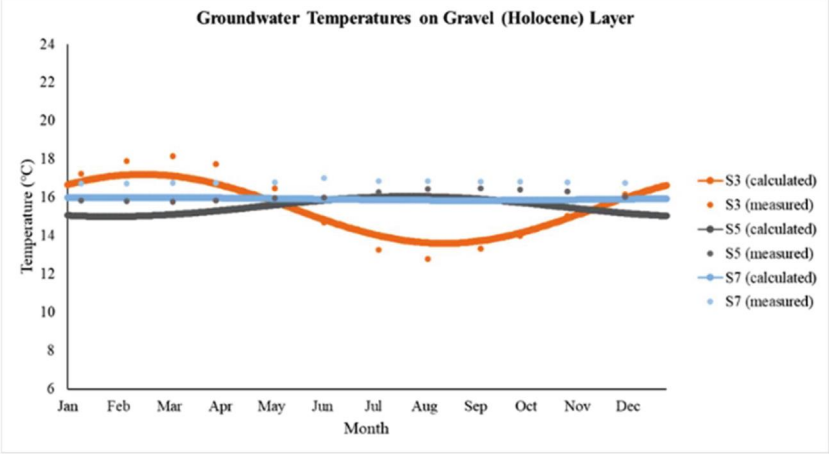
	3	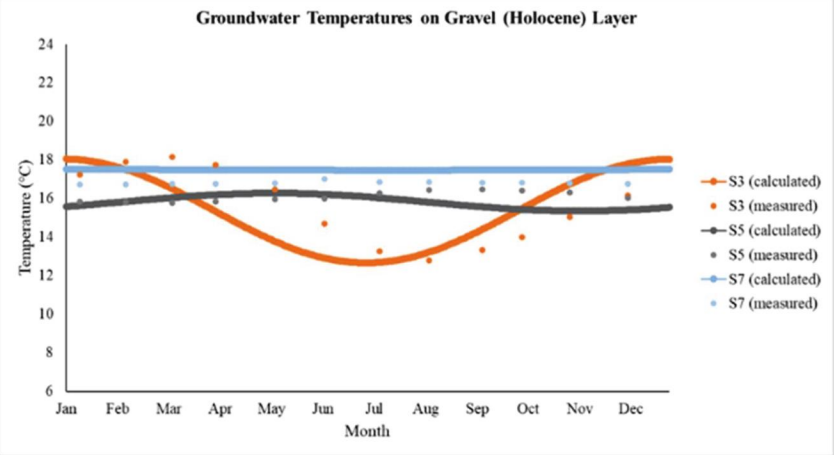

	4	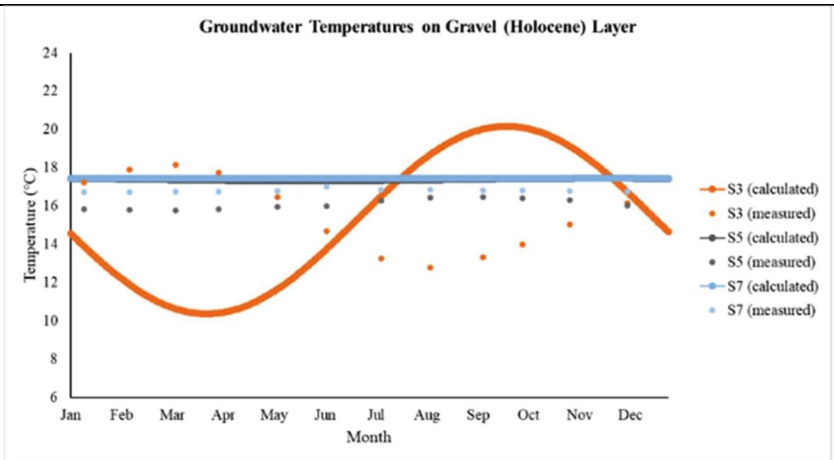

In Table 11 below are the values of the material properties of the flow and heat transport that are obtained after sensitivity analysis.

Table 11. Agreed material properties for flow and heat transfer for model simulation

Geological Layers	**Hydraulic conductivity (m/s)**	**Porosity (%)**	**Initial Temperature (℃)**	**Dispersivity**
Clay (Holocene)	$1x10^{-6}$	30	18	Longitudinal = 90 m Transverse = 9 m
Gravel (Holocene)	$7x10^{-2}$		16.3	
Gravel (Pleistocene)	$1x10^{-4}$			
Sand (Pleistocene)	$5x10^{-5}$			
Gravel (Pleistocene)	$1x10^{-4}$			
Chert, Sandstone, Shale (Jurassic Mino Accretionary Complex)	$1x10^{-8}$	10	18	

2.3.3 Local Model and Open-Loop Operation Settings

The local model is developed to evaluate the thermal impact of an open-loop GHP system. Figure 23 represents the construction of two local models. These locations were selected based on groundwater flow velocity. Local model 1 has a fast groundwater flow velocity, which is influenced by lateral flow recharged from the Nagara River and the hydraulic gradient. The local model 2 area has slow groundwater flow velocity and is located on the toe of the alluvial fan of the Nagara River. The local model boundary aligned to a hydraulic head contour line of the regional model. The hydraulic head and temperature boundary conditions were obtained from regional simulation results.

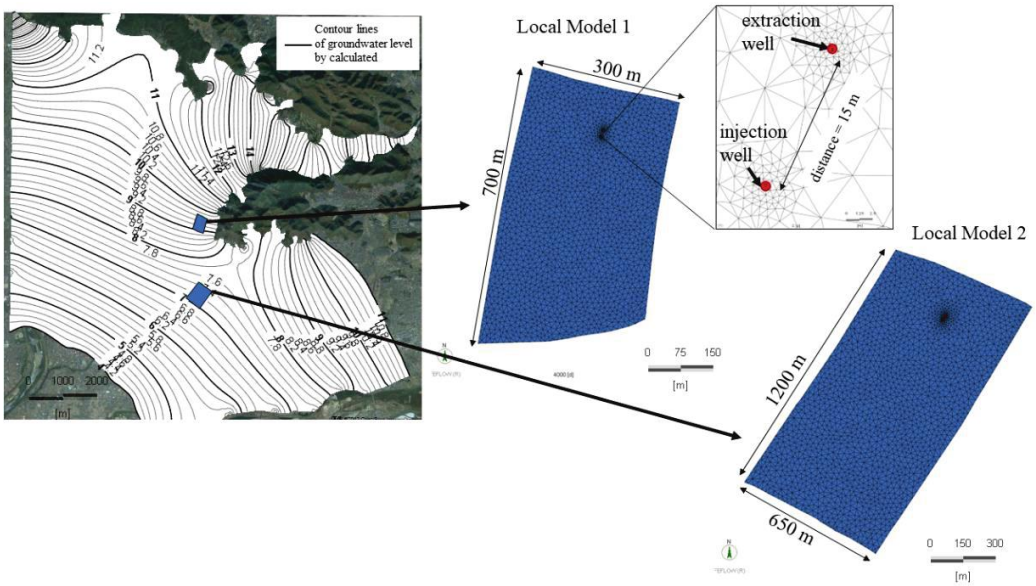

Figure 23. Local models 1 and 2

To evaluate the thermal impact of open-loop GHP system around the extraction and injection wells, the meshes of the local models were refined with finer meshes. Local models have been expanded to 3D local models with the same layer configuration as regional models (Figure 24). Local model 1 has dimensions of 300 m (EW), 700 m (NS), and 400 m (depth). Each slice has 1802 nodes (1 node per 8 m length and 1 node per 0.5 m length on the surrounding open-loop GHP system applied). Local model 2 had 650 m (NW-SE), 1200 m (NE-SW), and 400 m. (depth). There were 1831 nodes per slice (1 node per 15 m length and

1 node per 0.5 m length on the surrounding open-loop GHP system applied). The local simulation results were validated against the regional simulation results to ensure that the settings were correct. The open-loop GHP system was implemented in the local models after agreement.

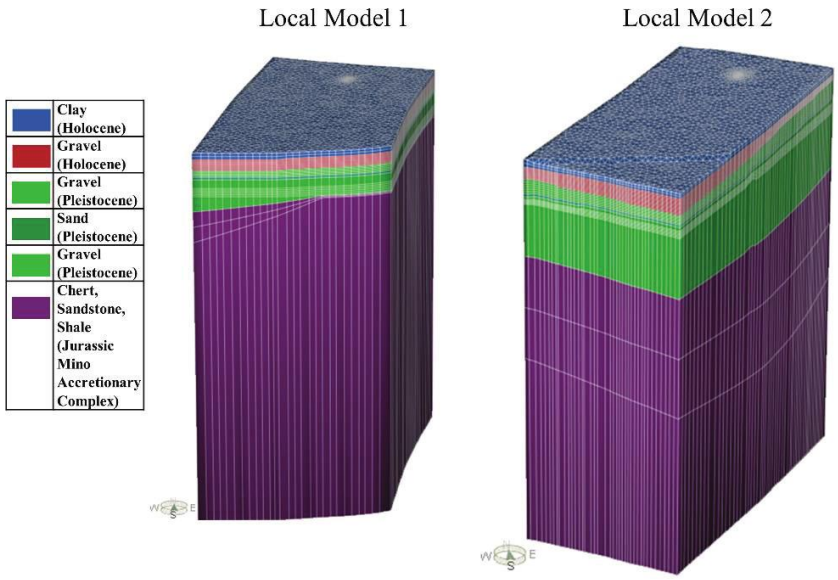

Figure 24. 3D Local Models 1 and 2

The 'Open-Loop Design plug-in' was used in FEFLOW to simulate the operation of open-loop GHP system. The open-loop system was designed with one extraction and one injection well separated by 15 m, with the extraction well situated upstream. The wells must be assigned using a variety of factors, including the pumping rate, well radius (0.15 m), and depth to the top and bottom of the well. Extraction and injection wells are screened with 10-15 m depth. According to this depth, they are located throughout the Holocene and Pleistocene gravel layers from 3–15 of the local model 1 and local model 2. The heating mode was used from January to March, and the cooling mode was used from July to September. For the cooling and heating periods of the open-loop GHP system, the groundwater temperatures were returned to the injection well with three variant values: 0, 5,

and 10 °C higher and lower than the extracted groundwater temperature. Pumping and injecting flow rates were 0 m^3/s (non-active), 3.33×10^{-3} m^3/s, 6.67×10^{-3} m^3/s, 1.67×10^{-2} m^3/s, and 3.33×10^{-2} m^3/s. Table 12 contains detail information of monthly pumping/injection rates and temperature difference for heating and cooling.

Table 12. Monthly pumping/injection rates and temperature difference for heating and cooling

Month	Pumping rate (m^3/s)	Temperature difference (°C)
January	3.33×10^{-3}, 6.67×10^{-3}, 1.67×10^{-2}, 3.33×10^{-2}	0, -5, -10 (from undisturbed temperature)
February	3.33×10^{-3}, 6.67×10^{-3}, 1.67×10^{-2}, 3.33×10^{-2}	0, -5, -10 (from undisturbed temperature)
March	3.33×10^{-3}, 6.67×10^{-3}, 1.67×10^{-2}, 3.33×10^{-2}	0, -5, -10 (from undisturbed temperature)
April	non-active	non-active
May	non-active	non-active
June	non-active	non-active
July	3.33×10^{-3}, 6.67×10^{-3}, 1.67×10^{-2}, 3.33×10^{-2}	0, +5, +10 (from undisturbed temperature)
August	3.33×10^{-3}, 6.67×10^{-3}, 1.67×10^{-2}, 3.33×10^{-2}	0, +5, +10 (from undisturbed temperature)
September	3.33×10^{-3}, 6.67×10^{-3}, 1.67×10^{-2}, 3.33×10^{-2}	0, +5, +10 (from undisturbed temperature)
October	non-active	non-active
November	non-active	non-active
December	non-active	non-active

CHAPTER 3: RESULTS

3.1 REGIONAL GROUNDWATER FLOW AND HEAT TRANSPORT RESULTS

The gradients of hydraulic head distribution obtained by measurement (upper left) and calculation (upper right) are displayed in Figure 25. The calculated and measured hydraulic head gradient directions as shown by red lines agree well. Both measured and calculated toward to the west. The hydraulic head level became lower toward the south for S1-S8 and lower to the west for N1-N8. The calculated results were almost consistent with measured in the observation points as we can see on Figure 25c.

Indeed, there is a discrepancy about 1 m between measured and calculated in the northern part. The calculated hydraulic head level is higher than the measured one in the northern part. These differences on hydraulic head levels are caused due to the settings of hydraulic head boundary condition. The hydraulic head boundary condition is set higher upstream of the Nagara River based on the Nagara and Akutami points. Consequently, there is an increase in hydraulic head in the north. On the other side, this change improves the southern hydraulic head. Because in some trials, the hydraulic head in the southern part is usually lower between about 1-2 m. Therefore, the hydraulic head results between calculated and measured is reasonably good.

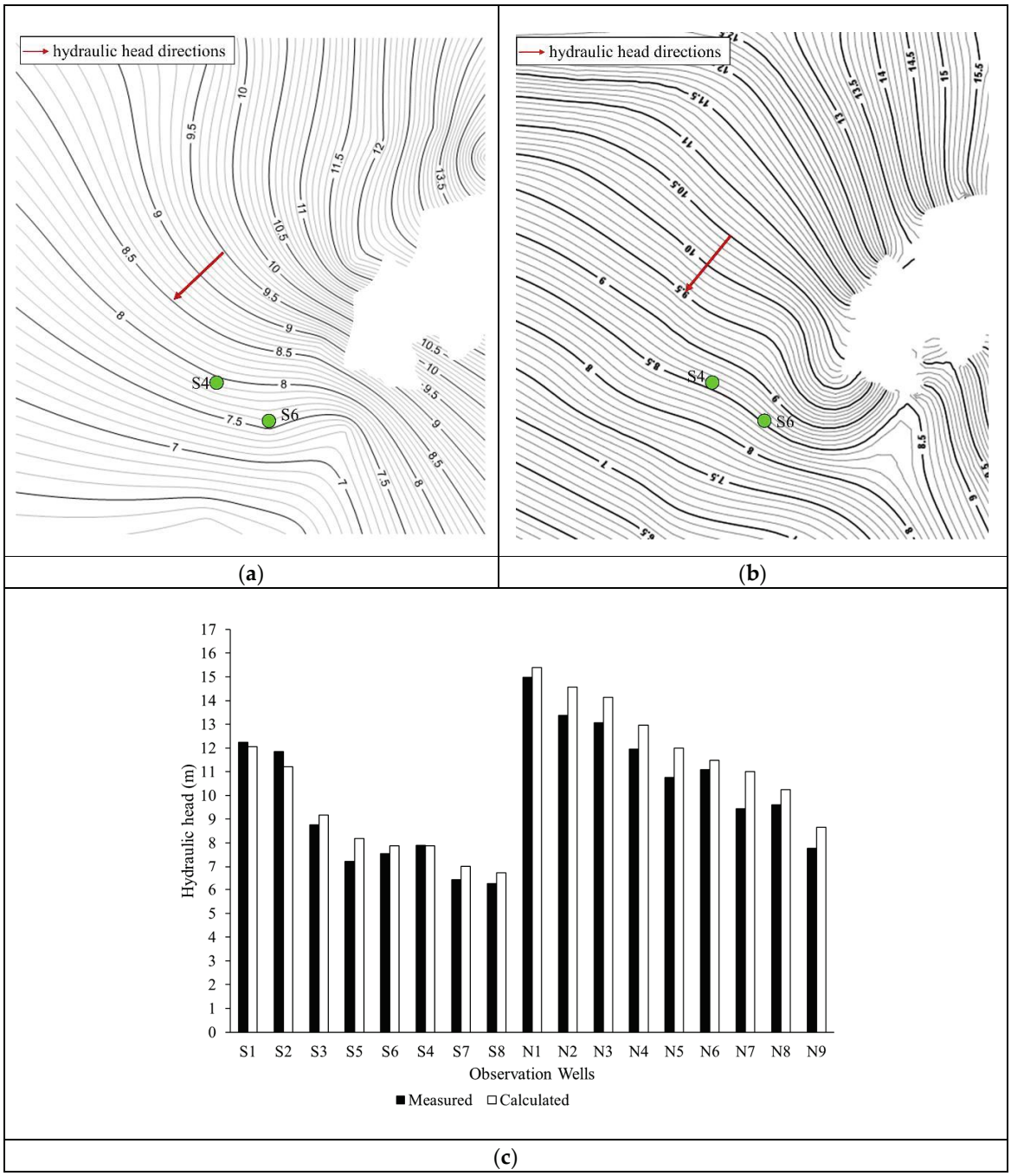

Figure 25. (**a**) Distribution of hydraulic head in the alluvial fan of the Nagara River by measured data (Ohtani et. al, 2015) (**b**) Distribution of hydraulic head in the alluvial fan of the Nagara River by simulation results, (**c**) Comparison of the hydraulic head between the calculated and measured data

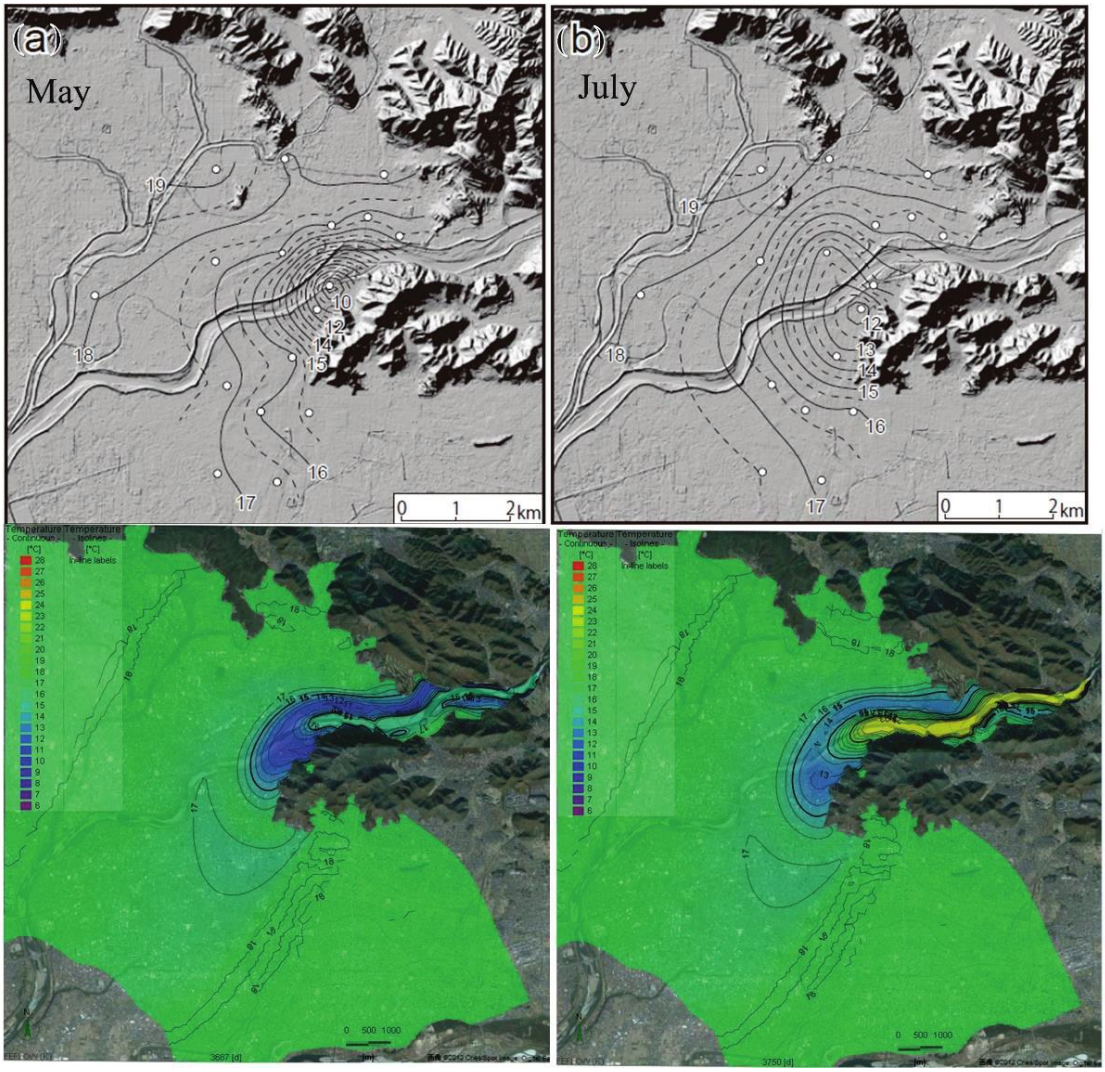
(a)
May
19
10
12
14
15
18
16
17
0 1 2km
(b)
July
19
12
13
14
15
16
18
17
0 1 2km
0 500 1000
0 500 1000

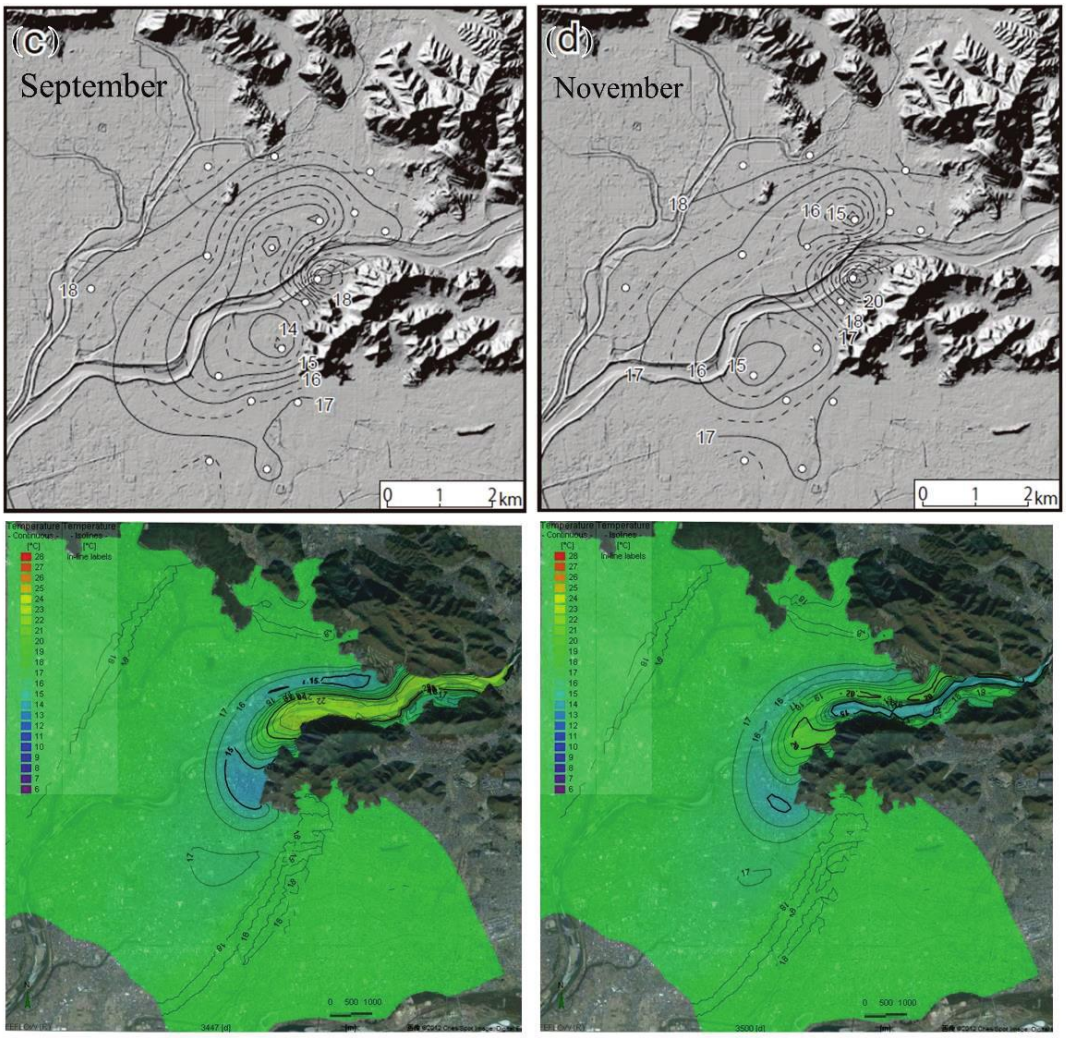
(c)
September
(d)
November
0 1 2km
0 1 2km

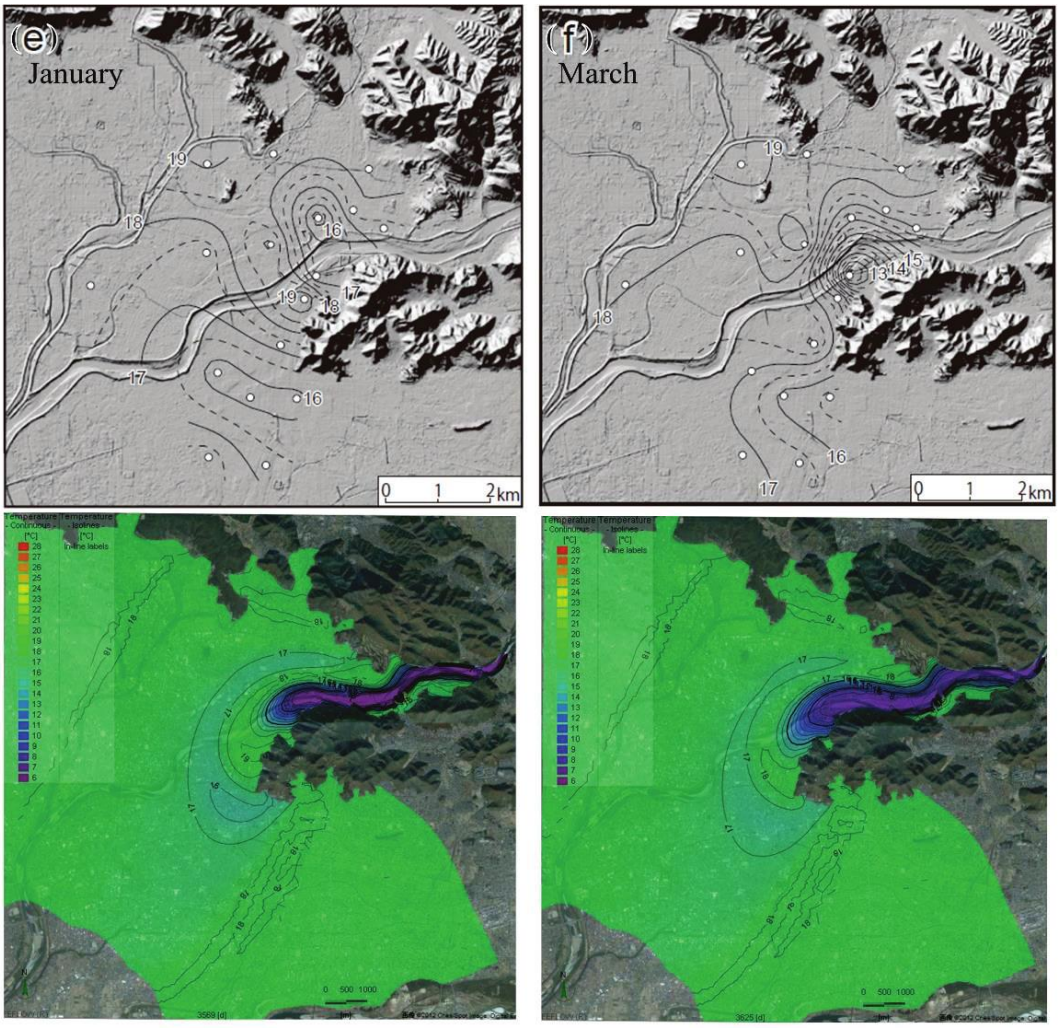

Figure 26. Regional groundwater temperature by measured (black and white; Ohtani et al., 2015) and calculated (color) results

Figure 26 depicts the distribution of groundwater temperatures in the Holocene gravel layer. The upper part shows the measured data (in black and white), and the lower parts are the simulation results (in color). The measured groundwater temperature distribution was obtained from the study of observation wells by Ohtani et al. (2015). The contour line of groundwater temperature between measured and calculated results from every two months has many similarities. This can be seen clearly by the similarities around Mount Kinka and confirmed by groundwater flow to the southwest of the alluvial fan. In May, the

groundwater temperature around the north of Mount Kinka is lower than that of its surroundings. The groundwater temperatures around the north of Mount Kinka rise in the summer (July and September) and falls in the winter (November, January, and March). The phenomenon of lateral groundwater flow from the apex to the toe of the alluvial fan can be described well with regional simulation results toward the south of each month's difference. However, it was discovered that there were discrepancies between the measured and calculated results in western areas. The groundwater temperature in the western area was shown around 16-17℃, while the calculated obtained 18℃. According to measured data, this discrepancy might be due to the fact that this area is still influenced by infiltrating water from the Nagara river. As a result, the groundwater temperature by measured is lower than calculated. Whereas in the simulation, this area tends to be stable because it is not influenced by the recharge zone as you can see from isoline. This difference may have been due to the limited number of observation wells in the measurement data. So, we cannot confirm this matter. Overall, these figures portray the activity of groundwater flow and heat transport in the simulated area. The model generally has well represented these phenomenon in the recharge of study area.

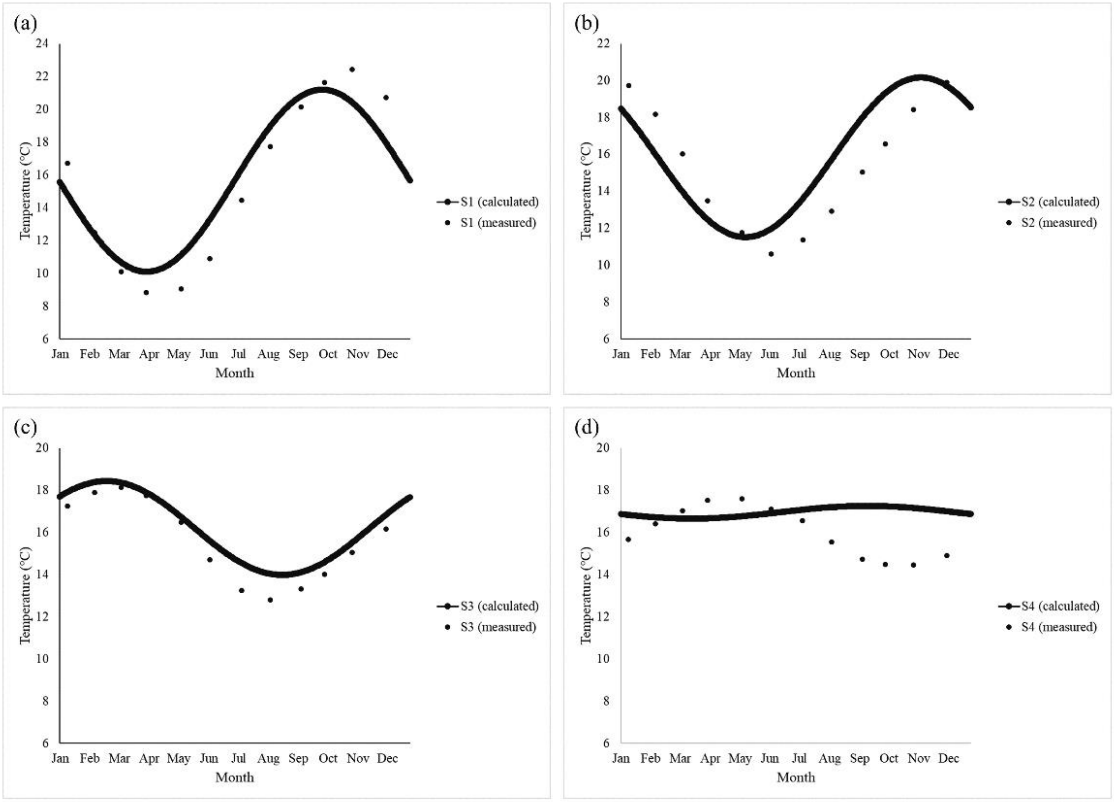
(a)
Temperature (°C)
Month
Jan Feb Mar Apr May Jun Jul Aug Sep Oct Nov Dec
S1 (calculated)
S1 (measured)
(b)
Temperature (°C)
Month
S2 (calculated)
S2 (measured)
(c)
Temperature (°C)
Month
S3 (calculated)
S3 (measured)
(d)
Temperature (°C)
Month
S4 (calculated)
S4 (measured)

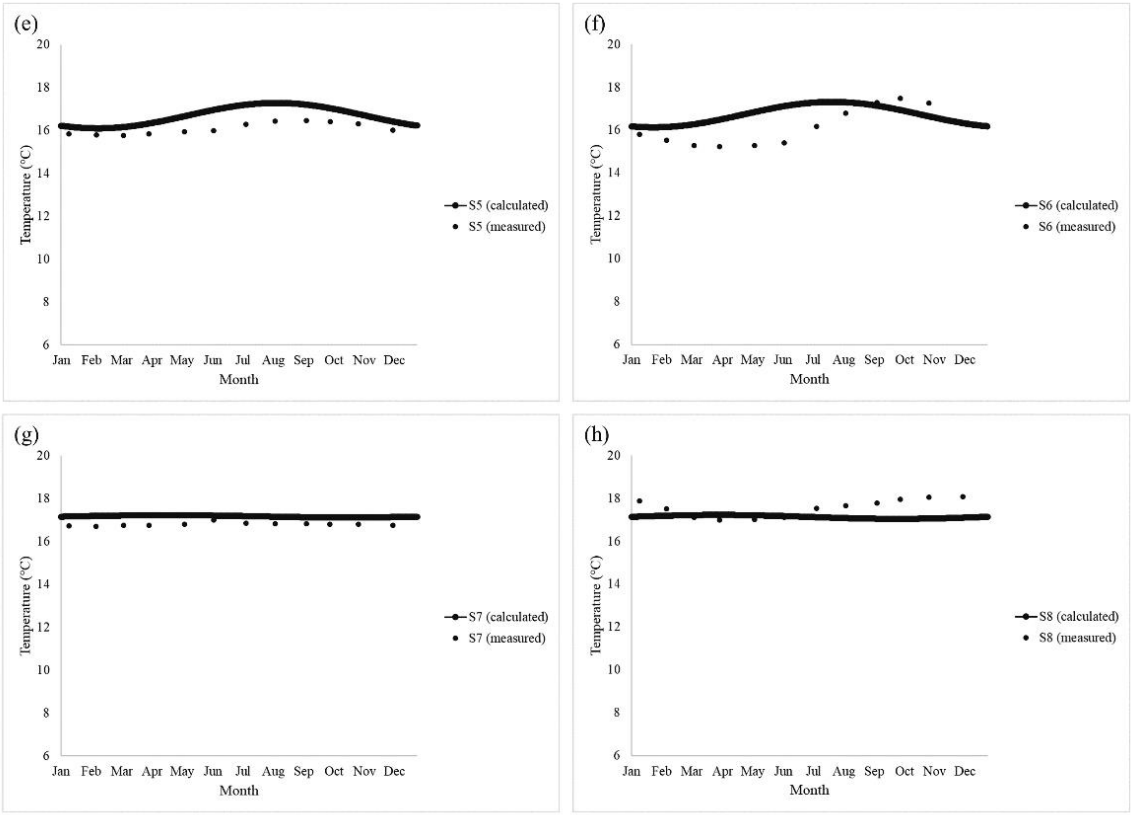

Figure 27. Comparison of the annual groundwater temperature change between the calculated and measured value at southern part on the Holocene gravel layer.

Figure 27 shows a comparison of the annual groundwater temperature changes in the 8 observation wells in southern parts between calculated and measured results in the Holocene gravel layer. As seen in Figure 27a–h, the calculated (smooth line) data are almost consistent with the measured (dot) data. However, there are noticeable differences between them on wells S4 (Figure 27d) and S6 (Figure 27f). We suspect this difference arose due to the slight difference in the hydraulic head gradient on Figure 25 on wells S4 and S6, thus slightly changing direction of groundwater flow. We assume that these changes affect the groundwater temperature in wells S4 and S6. This is also confirmed by the previous figure of the distribution of groundwater temperatures in Holocene gravels.

We also found that S1 and S2 observation points are also different. It is slightly noticeable that the groundwater velocity in the simulation is slightly faster than the measurement. The possibility of this difference arises in the different hydraulic conductivity of the Nagara River upstream and downstream. Therefore, we find that at observation points S3, S5, S7, and S8, there is good agreement between measurements and simulations. This is due to the fact that these areas are located downstream of the alluvial fan, which has a uniform hydraulic conductivity.

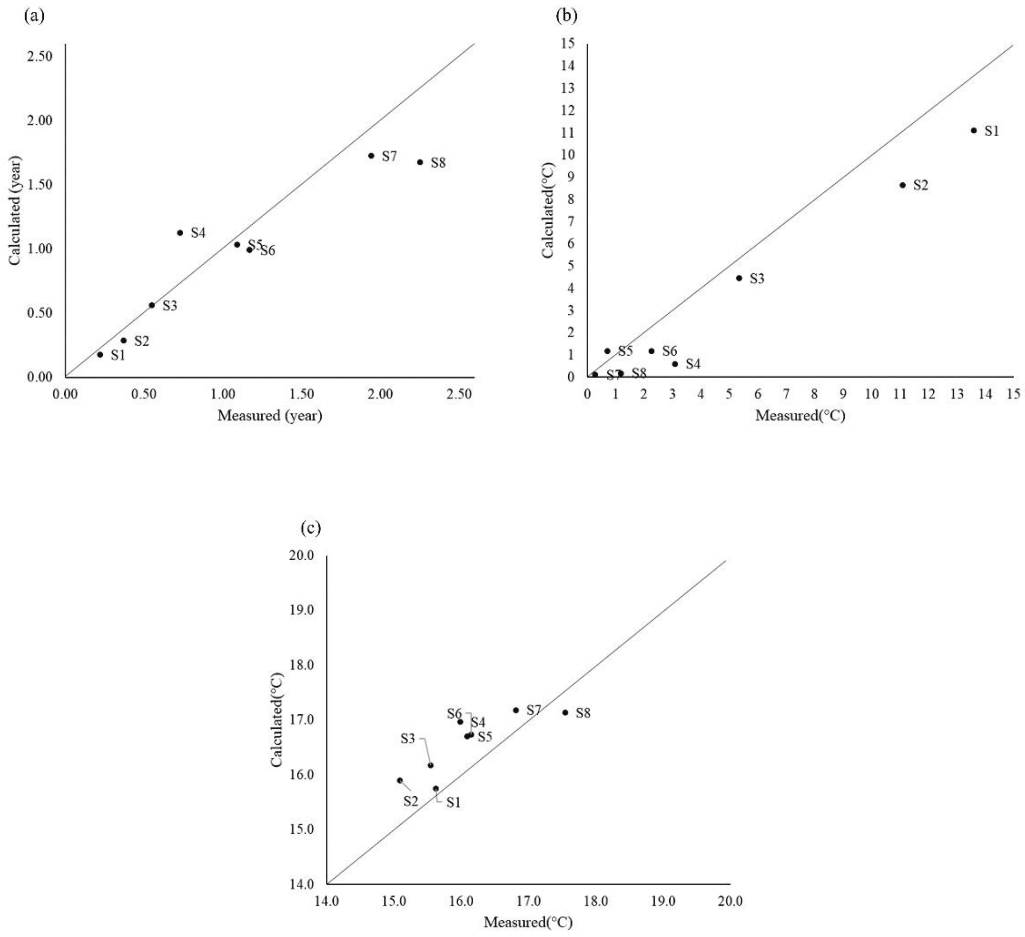

Figure 28. Phase difference (a), maximum-minimum (b), and average groundwater temperature (c) between measured and calculated on southern part.

The details of the phase difference, maximum and minimum groundwater temperatures, and average groundwater temperature are shown in Figure 28. The term "groundwater temperature change phase difference" in the well refers to the time difference between the outside air (recharge point of Nagara river) and the observation point as the temperature change cycle of waves in groundwater temperature. Observation points at wells S4 and S8 were non-linear from the graphs. Observation well S4 was different between measured and calculated presumably due to the slightly different lateral flow directions. The observation well S8 was non-linear because they almost had a constant groundwater temperature, so it was almost difficult to find the phase difference. It is called no phase difference.

The effect of different natural temperature changes at several observation points can also be seen from the graph of the max-min groundwater temperature change, where it is found that the measured data value is higher than the calculated one. In the graph of the average groundwater temperature, the natural temperature change of groundwater makes the average groundwater temperature value from the measured results lower than the calculated data. However, in general, the regional simulation has well-represented groundwater flow and heat transport, which are influenced by natural temperature change and lateral groundwater flow in the alluvial fan of the Nagara River.

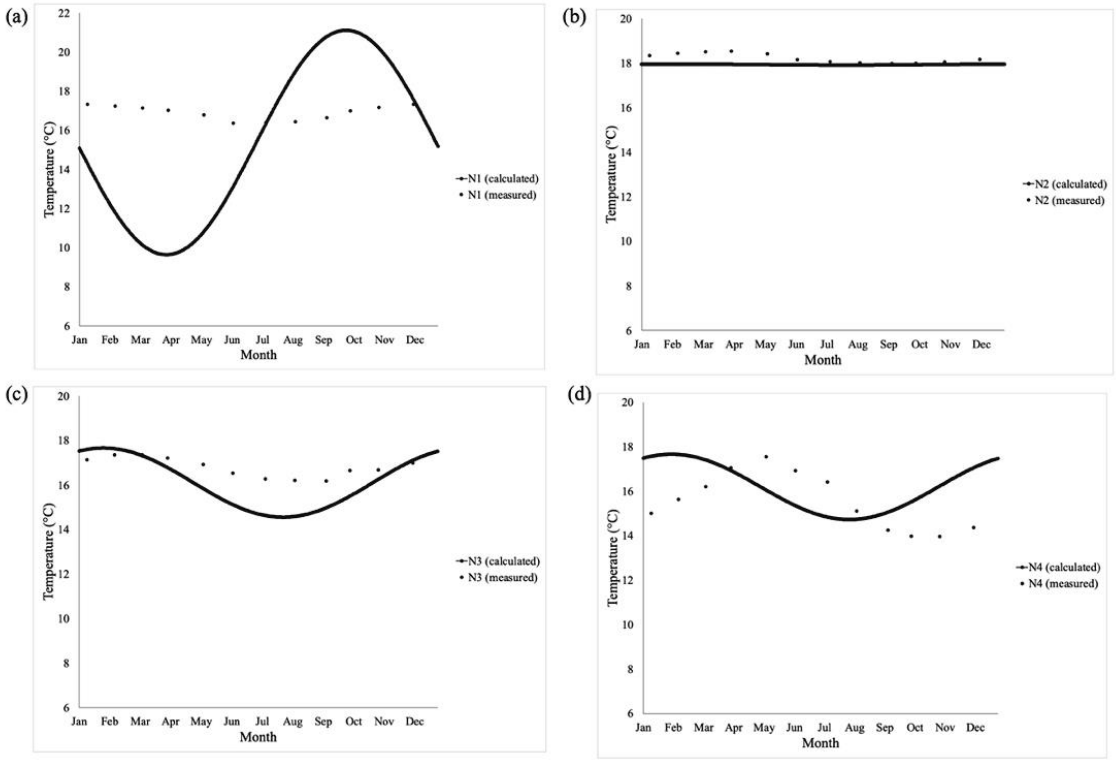
(a)
Temperature (°C)
Month
Jan Feb Mar Apr May Jun Jul Aug Sep Oct Nov Dec
N1 (calculated)
N1 (measured)
(b)
Temperature (°C)
Month
N2 (calculated)
N2 (measured)
(c)
Temperature (°C)
Month
N3 (calculated)
N3 (measured)
(d)
Temperature (°C)
Month
N4 (calculated)
N4 (measured)

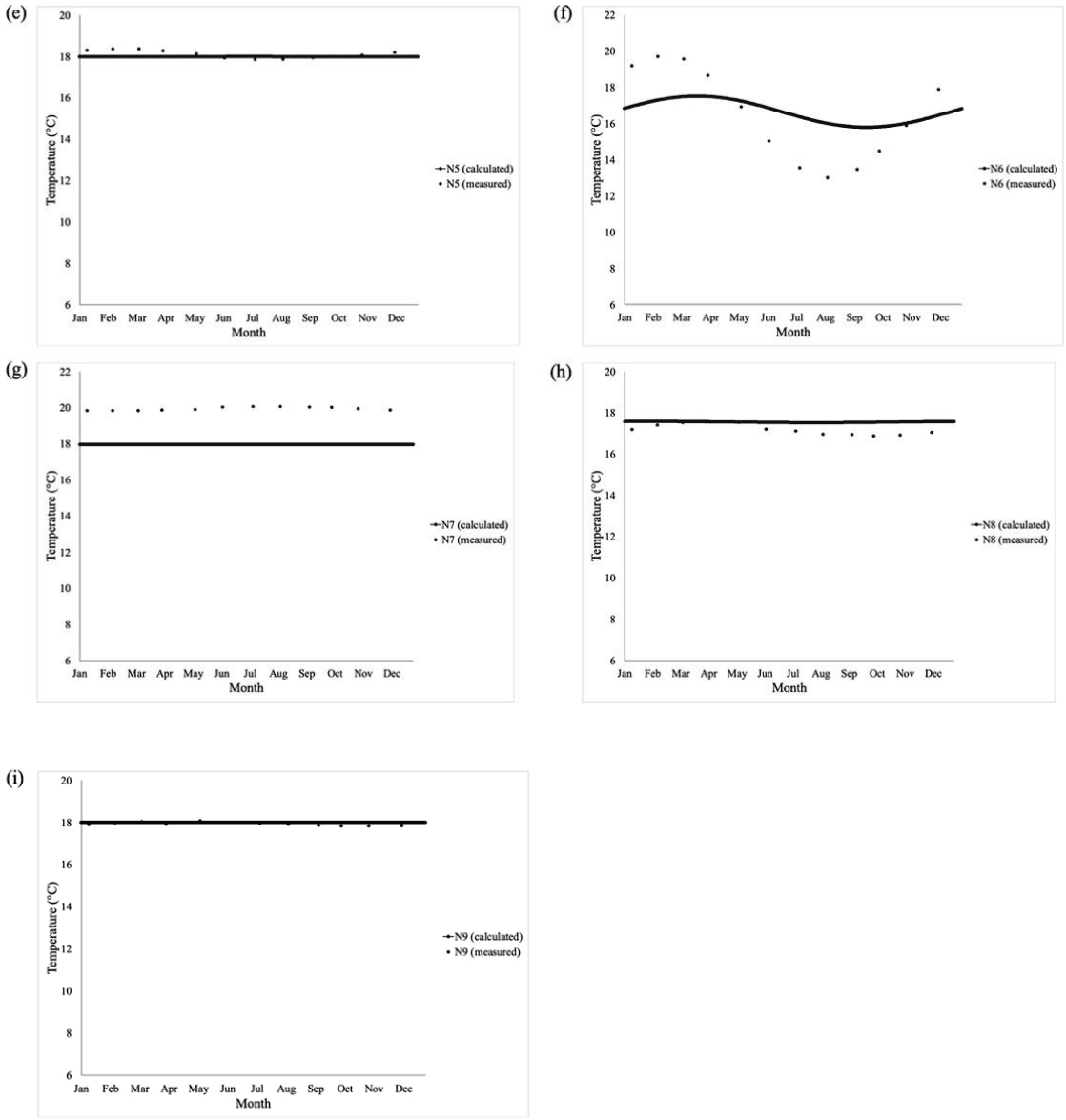

Figure 29. Comparison of the annual groundwater temperature change between the calculated and measured values northern part on the Holocene gravel layer.

In contrast to the southern side, the northern side's comparison of calculated and measured groundwater temperature data shows no similar patterns. Annual groundwater change on N1, N4 and N6 are noticeably different. As shown in Figure 29, calculated temperature data differ significantly from measured temperature data. Well N1 is located at

the apex of the alluvial fan closest to the estimated recharge area, followed by wells N2, N3, and so on. The matching annual groundwater change temperature between calcualted and measured is found at observation points that have a constant temperature, N2, N5, N8, and N9. As in the southern region, the calculated groundwater temperature show fluctuations near the recharge area and tend to be stable further away from the recharge area. On the other hand, most observation wells with measured data tend to be more stable in whole areas where the average measured temperature of the observation wells is higher than that of the river water temperature. The average annual measured temperature of the Nagara River is 15.2°C, while that of the groundwater in the northern side is 17.5°C. The difference between calculated and measured groundwater temperature of wells is greater than 2°C. It seems that the underground temperature at 15 m depth on the northern side is still influenced by the temperature at ground surface. The maximum temperature difference in the simulation grows larger toward the recharged zone in the southern area. The temperature and phase differences from observation wells on the northern side, on the other hand, produce non-linear graphs, as shown in Figure 30.

There is no relationship between lateral flow from the recharge area and groundwater temperature distribution in the northern side. This implies that the northern side has more complicated characteristics than the southern side. Ohtani et al. (2015) hypothesized that several recharge areas exist on the northern side. This was supported by evidence that this area included the channels of the ancient Nagara River. It is reasonable to assume that the old river channels have higher hydraulic conductivity than the other areas, and that the area with the greatest temperature difference is transmitted to the downstream side. Furthermore, the groundwater temperature in the northern area is affected by the river recharge of the Toba River, which is a tributary of the Nagara River.

Hydraulic conductivity was set to the same value in all horizontal directions for each type of soil/rock in this study. As a result, it was unable to represent the underground temperature change in the northern region by simulation, because the distribution of hydraulic conductivity with old river channels is complicated. It could be argued that

horizontal parameters should be set differently on the northern and southern sides in order to accurately represent the underground temperature change of the Nagara River fan.

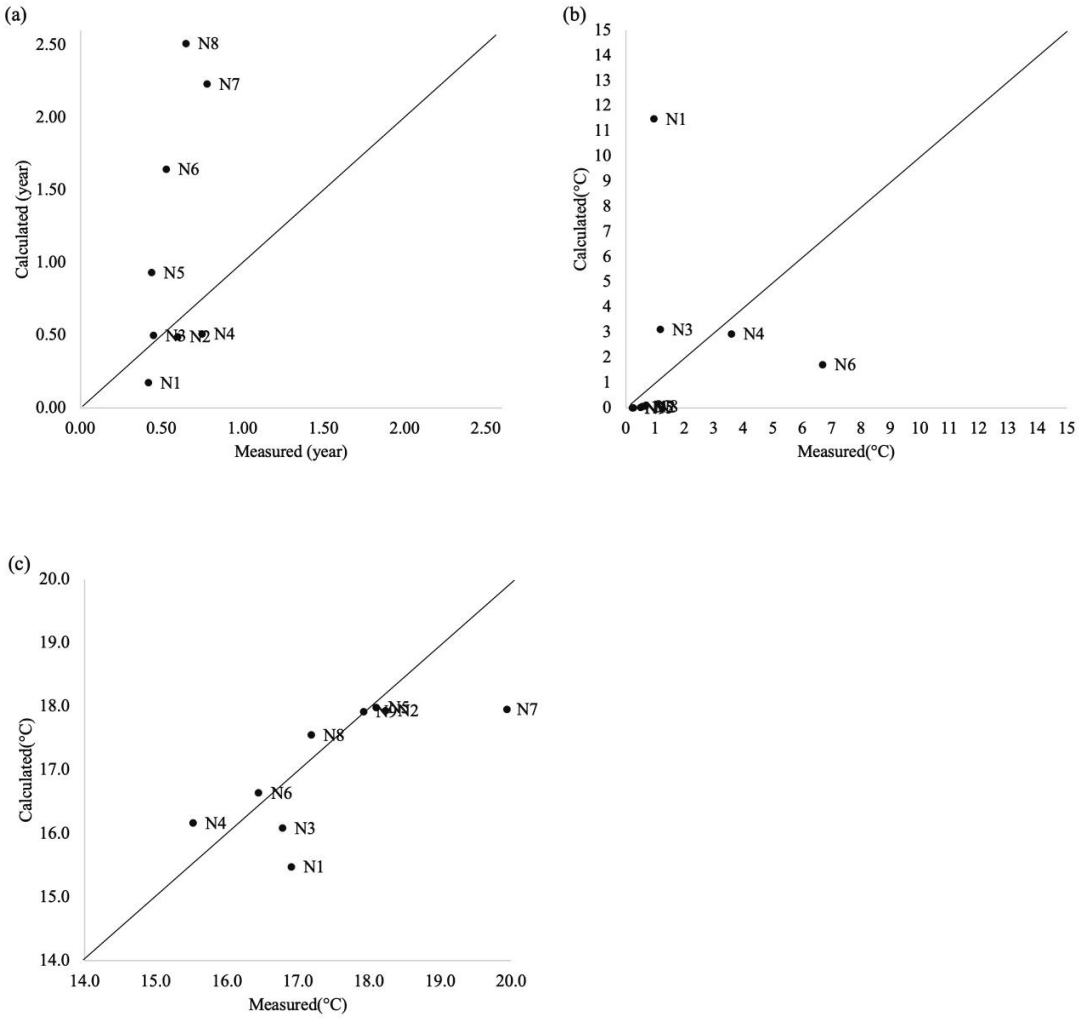

Figure 30. Phase difference (a), maximum-minimum (b), and average groundwater temperature (c) between measured and calculated on northern part

3.2 LOCAL SIMULATION AND OPEN-LOOP OPERATION RESULTS

The results of local simulations on 2 different models for thermal changes caused by heating and cooling operations are shown in Figures 31 and 32. The extent of thermal change and recovery after operation differed between the two local models. Due to the lateral groundwater flow, elongated areas with thermal changes were found in these two local models. Local model 1's elongated area was larger than local model 2's, as illustrated in Figure 31. However, due to the fast groundwater flow in local model 1, the thermal change recovered quickly after the heating and cooling operations. The recovery here means a return to a normal state of undisturbed groundwater temperature. Local model 2, on the other hand, as seen in Figure 32, required a long time to recover after heating and cooling. Even 90 days after the operation, thermal changes were still found in the downstream area. The open-loop system in local model 2 took longer to recover from the operation. Due to the slow groundwater flow, recovery was slower.

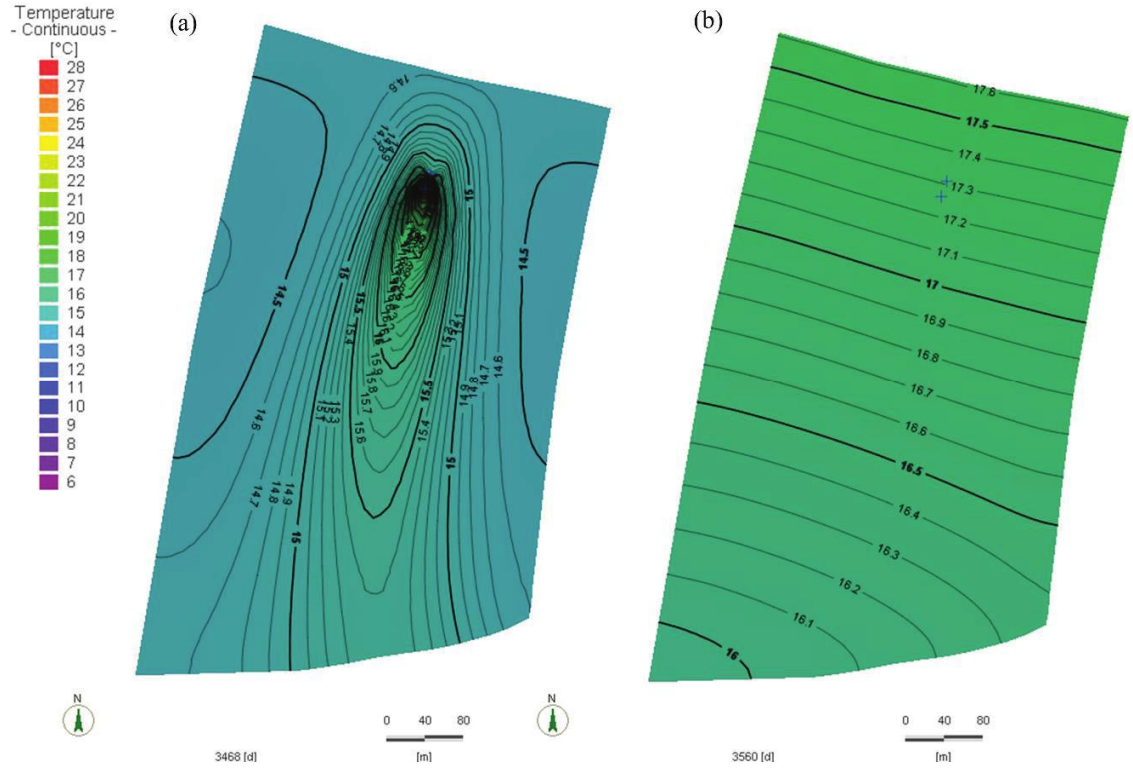

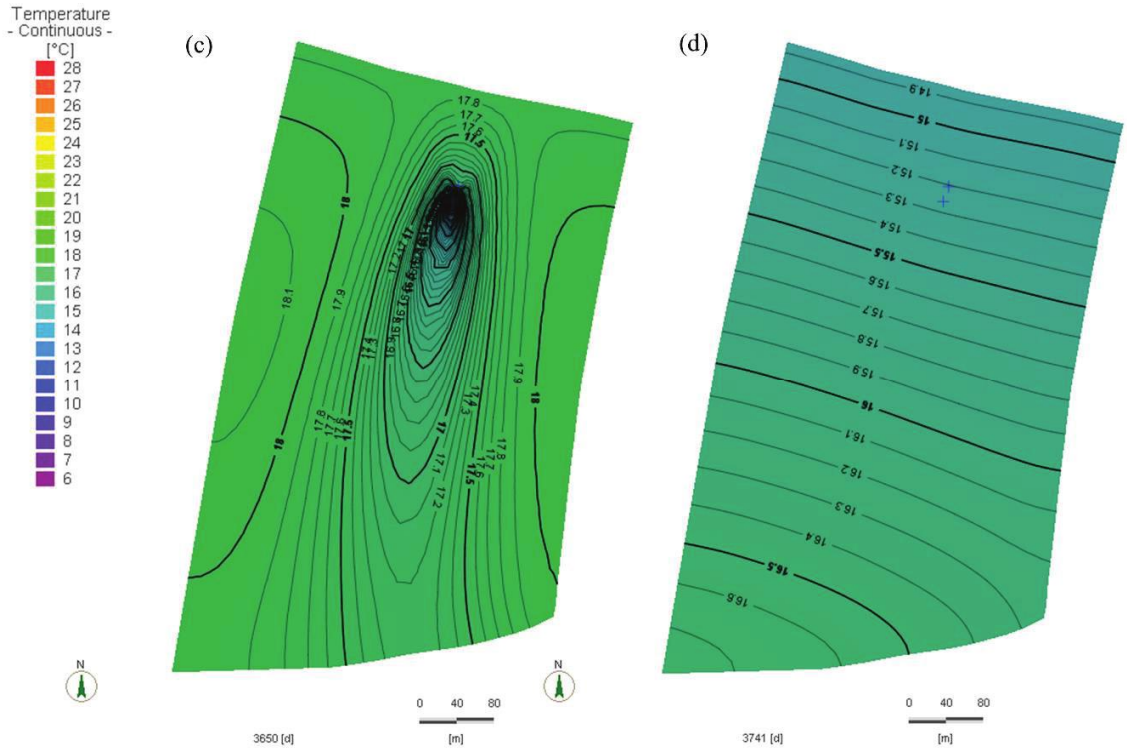

Figure 31. Thermal changes on variation VI (3.33×10^{-2} m^3/s, 10 °C) pumping rate 3.33×10^{-2} m^3/s and injection temperature 10 °C on local model 1, (a) during cooling operation, (b) after 90 days of cooling operation, (c) during heating operation, and (d) after 90 days of heating operation.

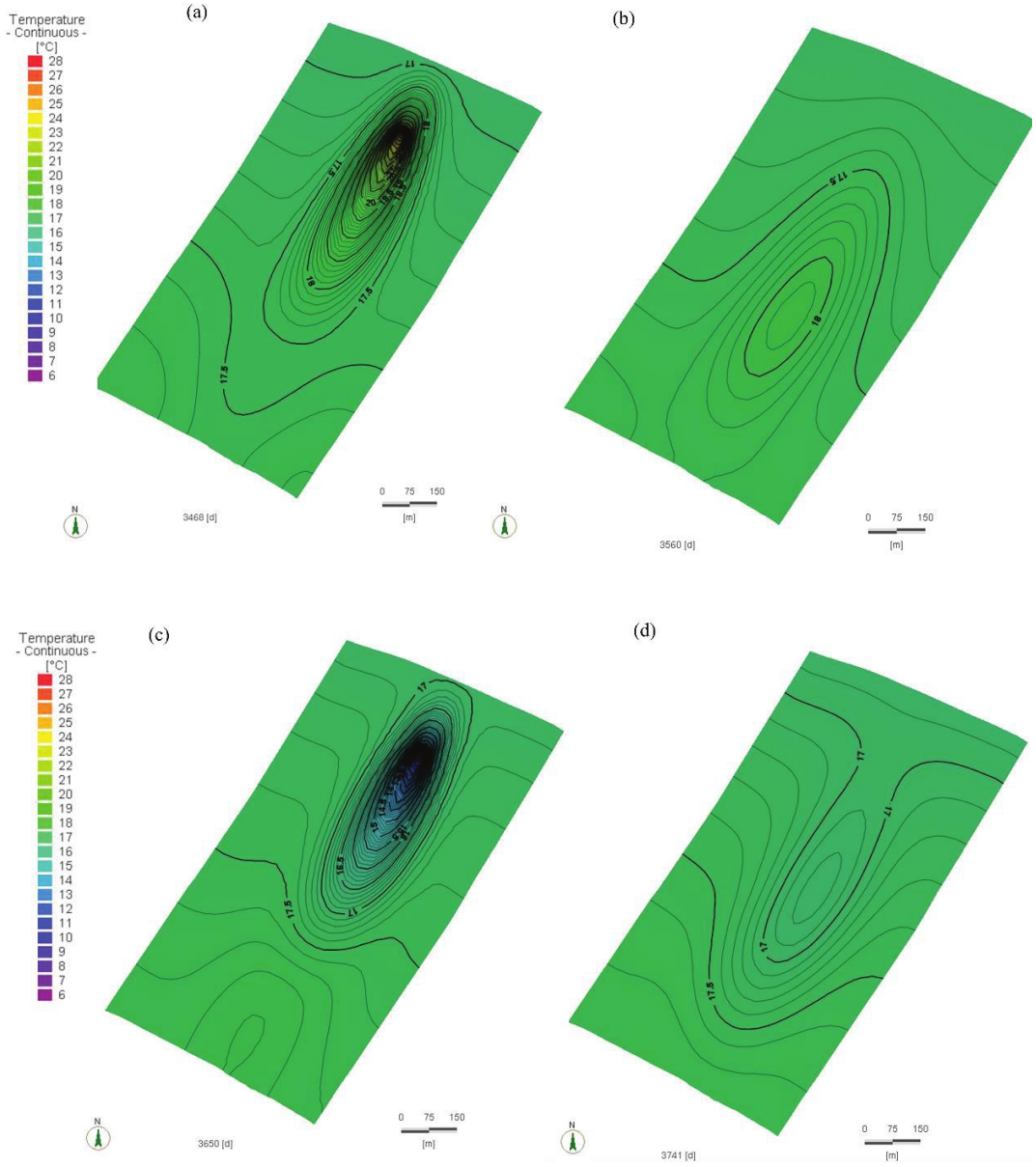

Figure 32. Thermal changes on variation VI (3.33×10^{-2} m^3/s, 10 °C) pumping rate 3.33×10^{-2} m^3/s and injection temperature 10 °C on local model 2, (a) during cooling operation, (b) after 90 days of cooling operation, (c) during heating operation, and (d) after 90 days of heating operation.

To examine the thermal environmental impact on the downstream area, we varied the pumping rate and injection temperatures. As shown in Figure 33, the 'non-active' indicates an inactive open-loop operation (0 m^3/s, 0 °C), while the variation I (3.33×10^{-3} m^3/s, 5 °C) shows a pumping rate of 3.33×10^{-3} m^3/s with a temperature difference of 5 °C, and so does the other variation. Figures 33 and 34 depict groundwater temperature changes due to open-loop GHP use in the downstream region at distances of 15, 30, 50, and 100 m from the injection well, with these variations.

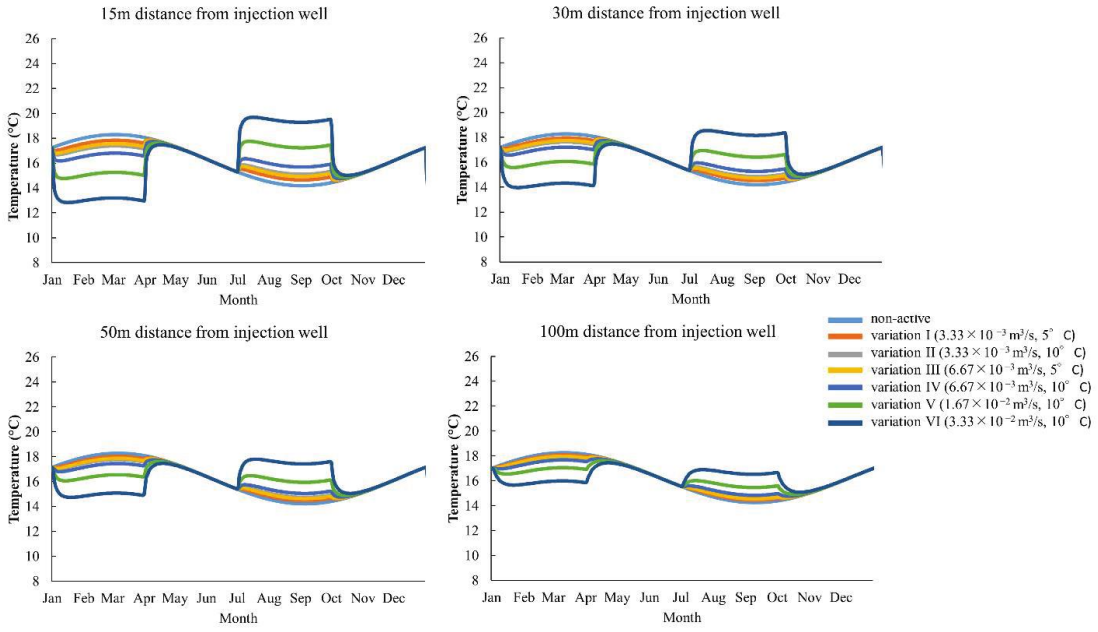

Figure 33. Thermal changes in local model 1 by open-loop GHP used in the downstream region at distances of 15, 30, 50, and 100 m from the injection well, with a variation of pumping rate and difference between the extracted and injected water temperature.

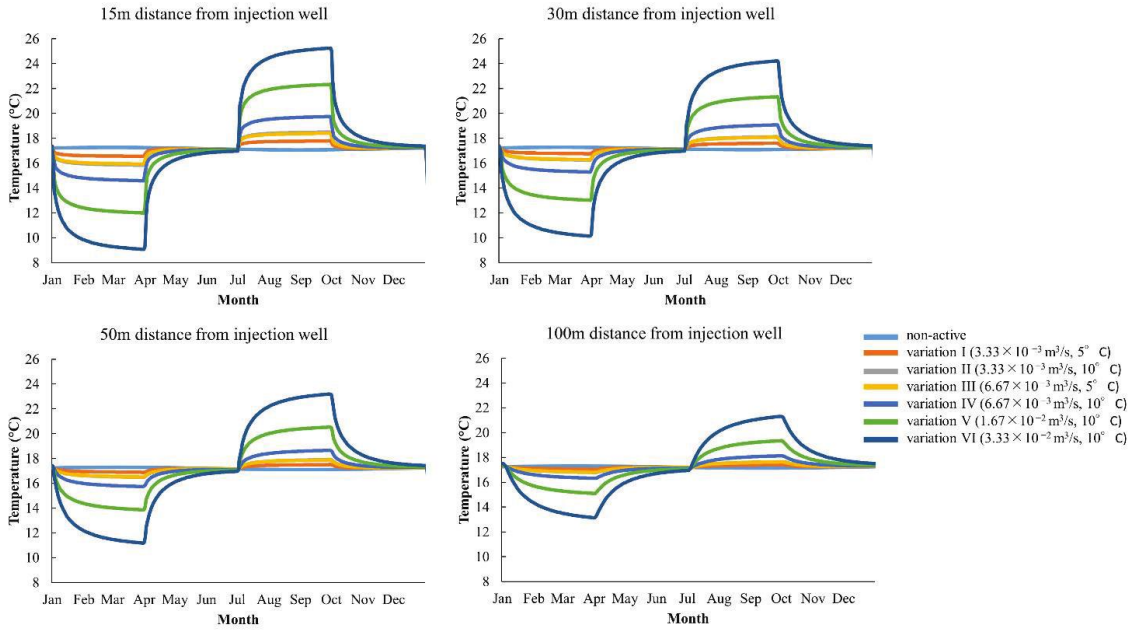

Figure 34.Thermal changes in local model 2 by open-loop GHP used in the downstream region at distances of 15, 30, 50, and 100 m from the injection well, with a variation of pumping rate and difference between the extracted and injected water temperature.

Overall, the thermal change decreased with the increased distance from the injection well. The largest temperature change in groundwater in local model 1 was 5 °C relative to non-active temperature using the highest variation, variation VI (3.33×10^{-2} m^3/s, 10 °C) at a 15 m distance from the injection well, whereas it was 7 °C in the local model 2. These results show that local model 1 has a lower temperature change than local model 2 at the same distance from the injection well. In local model 1, the thermal change due to open-loop system operation decreases faster than local model 2 due to faster groundwater flow as we can see at the same distance of 100m on Figure 33 and 34. Moreover, in local model 1, a slight slope of groundwater temperature change was found in the heating and cooling periods. This was caused by the effect of the natural temperature change of groundwater, where groundwater temperature was lower in summer and higher in winter. Therefore, the thermal change in local model 1 decreased slightly. As for model 2, thermal change continued to increase until the end of the period due to the small influence of natural changes in the

groundwater and slow groundwater flow. We also found differences after heating and cooling at the end of March and September, respectively. Local model 1 had a good ability to recover quickly compared to local model 2. Local model 2 requires a slightly longer time to the undisturbed groundwater temperature.

In addition, thermal changes could still be observed in the 450 m downstream area in local model 2, even after 90 days of heating and cooling operations. This situation gives the advantage of an open-loop system around a 450 m downstream area as groundwater temperature becomes lower in summer and higher in winter, as seen in Figure 35.

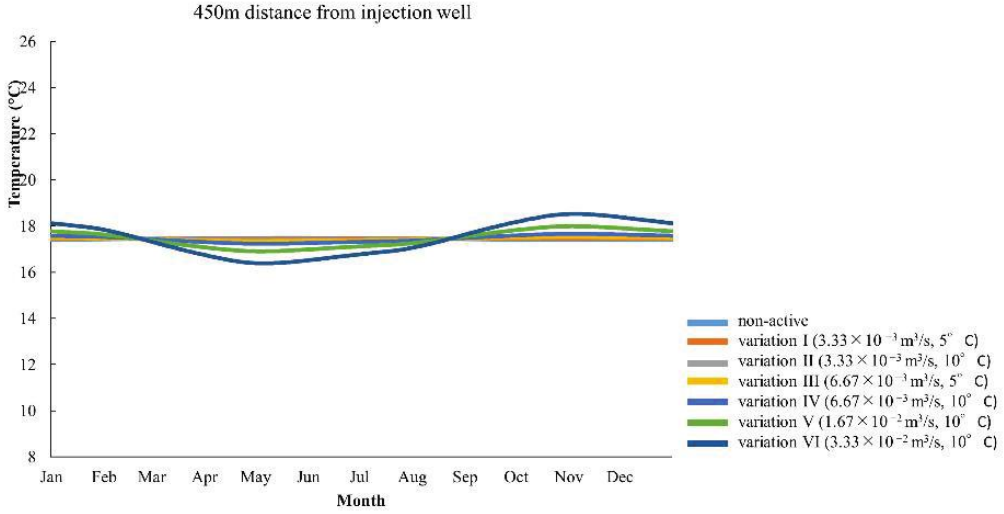

Figure 35. Thermal changes in local model 2 at 450 m distance from the injection well.

Figure 36 shows the groundwater temperatures of the extraction well at each variation in pumping rate and the difference between extracted and injected temperatures. The extraction well was 15 m upstream from the injection well. The increase in groundwater temperature around the extraction well was caused by an increase in the steepness of the mounds around the injection wells and the drawdown cones at the extraction wells. The higher the pumping rates applied, the greater the impact on the thermal feedback to the injection well. In this figure, we can also see that the impact of thermal feedback depends not

only on the pumping rate but also on the difference between the extracted and injected temperature. It was discovered that the impact of thermal feedback on the extraction well at variation II (3.33×10^{-3} m^3/s, 10 °C) was greater than that at variation III (6.67×10^{-3} m^3/s, 5 °C).

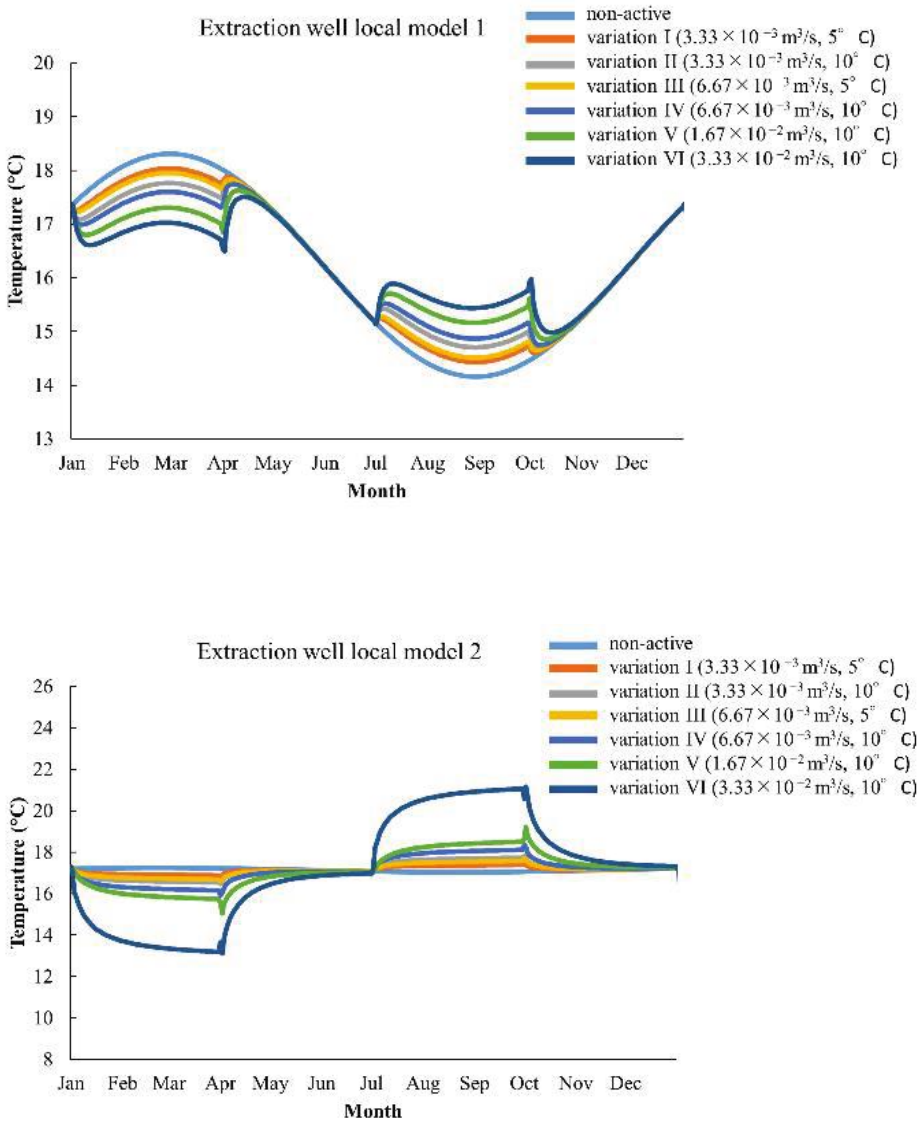

Figure 36. Groundwater temperature at extraction well on local models 1 (up) and local model 2 (down).

CHAPTER 4: DISCUSSION

4.1 REGIONAL SIMULATION

The calculated results of the regional simulation were almost consistent with the measured ones in the southern area. The hydraulic head of the groundwater became lower towards the south, and the heat in the aquifer was transferred towards the south in both the calculated and measured results. Although the calculated hydraulic heads show a small discrepancy from the measured ones, this small difference is acceptable due to the following reasons: First, the hydrological data used for the hydraulic head boundary conditions were derived from water level measurements taken at 195 observation wells in February 20-21, 2014, while the measured data used as a comparison was derived from the annual average groundwater level value by Ohtani et al. (2015). Second, the hydraulic head boundary condition is set higher upstream of the Nagara River based on the Nagara and Akutami points. As a result, the hydraulic head in the northern section increases. However, this modification improves the southern hydraulic head. Considering that in some trials the hydraulic head is often lower in the southern region around 1-2 m and the limited observation points in this vicinity. Third, the boundary condition of the hydraulic head was constant, and the transient flow was not treated in this study.

Based on groundwater temperature results, the comparison between calculated and measured data has almost good correlation at southern region of model. Temperature difference and phase difference between calculated and measured data display almost linear graph. Unlike the southern part, the comparison of calculated and measured groundwater temperature data in the northern side of Nagara River do not have similar patterns. Calculated temperature data are noticeably different from the measured ones. This is due to two factors. First, the groundwater flow velocity is higher in areas that are closer to the recharge area and lower far further away. The parameter of the hydraulic conductivity of the Holocene gravel layer was a constant value, and it was, therefore, different from the actual setting. Neton et al. (1994) described the horizontal heterogeneity of the hydraulic conductivity of the aquifer in the alluvial fans and introduced the down-fan fining trend, trending heterogeneity, and

humped heterogeneity. Although the alluvial fan of the Nagara River is distributed along the margin of the Nobi Plain, the river has several basins on its upstream side, and debris flows do not reach this alluvial fan. This suggests that the distribution of hydraulic conductivity in the Holocene gravel layer shows the down-fan fining trend. Second, it suggests the presence of several recharging areas in northern areas. The distribution of basement rocks in the northern cause a lower permeability. Therefore, river water cannot infiltrate the aquifer on the northern part. Therefore, the groundwater temperature here tends to be stable.

4.2 COMPARISON BETWEEN LOCAL MODELS 1 AND 2

This study showed the thermal impact of the open-loop geothermal system with local model 1 with faster groundwater flow, influenced by a natural change in the groundwater system and local model 2 with slower groundwater flow, influenced by a very small natural change in the groundwater system. The differences in the calculated results on the thermal impact between the local models were the maximum thermal change from the natural one, the recovery period after the heating/cooling operation, and the temperature change during the heating/cooling operation.

The maximum thermal change from the natural one in local model 1 was 5 °C and that in the local model 2 was 7 °C in the case of variation VI, which had a 3.33×10^{-2} m^3/s pumping rate and a 10 °C temperature difference between the extraction and injection water. The recovery period for local model 1 was about 15 days after the operation, whereas for local model 2, it took more than 90 days to reach an undisturbed groundwater temperature. The temperature change during the heating and cooling operations on local model 1 slightly decreased, whereas, on local model 2, thermal change continued to increase until the end of the operation period. The results of the first two came from the difference in the groundwater flow velocity, and the third results were from the fast groundwater flow and the existence of the natural temperature change. The thermal impact of local model 1 was lower than that of local model 2. This means the open-loop system can be installed densely in an area with rapid groundwater flow.

The thermal impact of local model 2 is not negligible for geothermal use on the downstream side. Previous studies also mention this point. For example, Meng et al. (2019) examined the thermal impact and long-term sustainability of the GHP that is used on a small scale in the alluvial fan area where vertical groundwater temperature variation is roughly 0.15°C. It has been demonstrated through long-term simulations that the accumulation of cold plumes caused by heating occurs in the downstream area. The cold accumulations were carried out by many installations in the upstream region. Downstream installations were found unsustainable from the economic aspect due to the consumption of more electrical energy and a lower.

In this research, we conducted several numerical experiments by varying the pumping rate with the injection temperature to determine the maximum thermal change. According to Freedman et al. (2012), the higher pumping rate and lower injected water temperature resulted in smaller thermal plumes in the downstream area. This is consistent with our finding that variation II has a greater thermal impact (3.33×10^{-3} m^3/s, 10 °C) than variation III (6.67×10^{-3} m^3/s, 5 °C). However, the higher pumping rate resulted in higher thermal feedback at the extraction well, where the extraction well was a distance of 15 m from the injection well. The 15 m distance was less than the ideal distance for minimizing thermal feedback in local model 2, but it was acceptable in local model 1. The pumping rate was 3.33×10^{-3} m^3/s with water injected at a temperature difference of 5 °C or 10 °C higher or lower than the extracted groundwater temperature. The 10 °C temperature difference of injected water caused higher thermal plumes in the downstream area since the increase in injected water temperature into the injection well must be considered for its impact on the downstream area.

However, Freedman et al. (2012) and Meng et al. (2019) studied the thermal impact in areas without natural temperature change. The alluvial fan of the Nagara River has rapid groundwater flow and is influenced by natural groundwater temperature change. These conditions are advantageous for the sustainability of the GHP system. The COP of the heat pumps depends on the groundwater temperature. In cooling, the lower the groundwater temperature, the more efficient and economical the heat pump operates. Natural temperature

change in the alluvial fan of the Nagara River causes local model 1 groundwater temperature to be lower in summer and higher in winter (Figure 27c). Therefore, open-loop GHP in this area becomes more efficient. The thermal impact of local model 1 is lower than that of local model 2. This means the open-loop system can be installed densely in an area with rapid groundwater flow. A lower pumping rate can also be applied with a higher injected water temperature on local model 1 for a higher SCOP (Seasonal Coefficient of Performance), because the higher injected water temperature is still sustainable for the downstream area.

CHAPTER 5: CONCLUSION

Regional and local simulations of groundwater flow and heat transport were developed to determine the distribution of groundwater flow velocity and temperature and to assess the thermal environmental impacts of an open-loop GHP system in the alluvial fan of the Nagara River, Gifu City, Central Japan. Based on regional simulation result, the comparison between calculated and measured data has almost good correlation at southern region of model. Temperature difference and phase difference between calculated and measured data display almost linear graph. On the other hand, there are noticeable difference between calculated and measured data at northern region. In addition, temperature difference and phase difference also showed nonlinear graph. This indicates the presence of several recharge areas. Furthermore, the northern area is surrounded by mountains. Since the permeability of the bedrock is lower, it is possible that river water cannot infiltrate the aquifer. So, the groundwater temperature tends to be stable and has no correlation with the natural change of groundwater from the Nagara River. The model was constructed by not considering those kinds of factors due to limited data.

The local simulation of open loop GHP system results showed that local model 1 with a fast groundwater flow velocity had a less thermal impact than local model 2 with a slow groundwater flow velocity. Because of the presence of natural temperature change, the local model 1 groundwater temperature is lower in the summer and higher in the winter during operation. As a result, the thermal impact of local model 1 gradually decreases relative to that of local model 2 while the open-loop GHP system is operating. Due to the fast groundwater velocity, the thermal change by operating open-loop GHP of local model 1 is relatively smaller than that of local model 2. Furthermore, thermal change of local model 1 recovers faster than local model 2. After 90 days of heating and cooling, the groundwater temperature distribution in local model 1 restored to normal. In local model 2, thermal changes were still seen downstream in the 450 m distance. This situation, on the other hand, makes this zone suitable for regional thermal energy storage since the groundwater temperature in this zone is slightly cooler in the summer and slightly warmer in the winter.

Rapid groundwater flow and natural temperature changes in groundwater give better efficiency and reduced thermal impact benefits for the open-loop GHP system. This research is particularly useful for modeling the possible thermal impact of open-loop GHPs in areas such as the Nagara River alluvial fan with fast groundwater flow velocity. The distance between individual installations may be evaluated to determine whether thermal feedback occurs, and long-term sustainability, particularly in the downstream area, can be checked to see if several systems are utilized in the upstream area. This simulation can be used in regional conditions with a similar range of parameter values as the study area in the alluvial fan.

This research can be considered before installing an open-loop system in the alluvial fan of the Nagara River because it allows us to evaluate the thermal impact of open-loop GHP system use and its impact on the surrounding area or nearby installation. The simulation model is not limited to the alluvial fan of the Nagara River, but it can be applied to a variety of alluvial fan areas as long as the parameter values are within the same range. After several sensitivity analyses, the values of hydraulic conductivity, pumping rate, initial temperature and dispersivity were determined to be the most sensitive parameters. These values can determine the application of the study in the alluvial fan area. The alluvial fan of the Nagara river is influenced by infiltration processes and rapid groundwater flow recharged from the river. Due to these circumstances, natural changes in river water temperature and lateral groundwater flow impact the groundwater temperature.

In addition, if multiple applications of the GHP system are installed upstream in local model 2, this will have a thermal impact on its downstream areas. More installations in the downstream area of local model 2 would make it unsustainable, and its groundwater temperature would be greatly affected. This condition, on the other hand, is advantageous for the downstream area at 450 m. We can take this condition into use by implementing artificial thermal energy storage (ATES) where many installations in the upstream area provide thermal benefits in the downstream area. In summer, the groundwater temperature is relatively cold around 450m due to the thermal impact of the upstream open-loop GHP

system. This cold groundwater was extracted to be used as air conditioning. After 6 months, the temperature of the groundwater will reverse to become warmer. We extract the warm temperature of the groundwater to warm the building. To obtain a better understanding of these effects, it may be necessary to conduct simulations over a longer time period, such as several years. This would allow for a more thorough evaluation of the potential impacts and help inform decisions related to the design and management of the system.

Acknowledgements

Special thanks to the City of Gifu for providing borehole data.

Additionally, I would like to express my sincere thanks for the remarks and guidance given by Prof. Tomoyuki Ohtani, Prof. Satoru Kojima and Prof. Kohji Kamiya. To my advisor Professor Tomoyuki Ohtani, he has been a tremendous mentor for me. I would like to thank you for encouraging my research and for allowing me to grow as a research scientist, for his patience, motivation, enthusiasm, and immense knowledge. His advice on both research as well as on my career have been priceless. To Professor Satoru Kojima, he has instructed and helped me a lot in the past 5 years, giving me the hard question to widen my knowledge from different perspective during my study and for letting my study be enjoyable moment, and for your brilliant comments and suggestions. I would like to express my gratitude to Naoko Yamada for her help with administrative tasks during my master and PhD. My appreciation to Vital and Auxilio for being my first foreign friends in the laboratory. My special thanks were given to members in Earth Science Laboratory from 2017 to 2022.

I would also like to thank the AGP Program and the Department of Engineering Science for giving me the opportunity to pursue my doctoral degree with AGP scholarship at Gifu University.

REFERENCES

Bayer, P., Saner, D., Bolay, S., Rybach, L., Blum, P., 2012. Greenhouse gas emission savings of ground source heat pump systems in Europe: A review. Renew. Sustain. Energy Rev. 16, 1256–1267. https://doi.org/10.1016/j.rser.2011.09.027

Bonte, M., Stuyfzand, P.J., Van Den Berg, G.A., Hijnen, W.A.M., 2011. Effects of aquifer thermal energy storage on groundwater quality and the consequences for drinking water production: A case study from the Netherlands. Water Sci. Technol. 63, 1922–1931. https://doi.org/10.2166/wst.2011.189

Brielmann, H., Griebler, C., Schmidt, S.I., Michel, R., Lueders, T., 2009. Effects of thermal energy discharge on shallow groundwater ecosystems. FEMS Microbiol. Ecol. 68, 273–286. https://doi.org/10.1111/j.1574-6941.2009.00674.x

Bulté, M.; Duren, T.; Bouhon, O.; Petitclerc, E.; Agniel, M.; Dassargues, A., 2021. Numerical Modeling of the Interference of Thermally Unbalanced Aquifer Thermal Energy Storage Systems in Brussels (Belgium). Energies 14, 6241. https://doi.org/https://doi.org/10.3390/en14196241

Casasso, A., Sethi, R., 2015. Modelling thermal recycling occurring in groundwater heat pumps (GWHPs). Renew. Energy 77, 86–93. https://doi.org/10.1016/j.renene.2014.12.003

Chi-Yuen Wang, M.M., 2021. Water and Earthquakes. Springer, Cham. https://doi.org/https://doi.org/10.1007/978-3-030-64308-9

Diersch, H.-J.G., 2014. FEFLOW Finite Element Modeling of Flow, Mass and Heat Transport in Porous and Fractured Media. Springer-Verlag Berlin Heidelberg 2014, Berlin, Germany. https://doi.org/DOI 10.1007/978-3-642-38739-5

Freedman, V.L., Waichler, S.R., Mackley, R.D., Horner, J.A., 2012. Assessing the thermal environmental impacts of an groundwater heat pump in southeastern Washington State. Geothermics 42, 65–77. https://doi.org/10.1016/j.geothermics.2011.10.004

Fujii, H., Inatomi, T., Itoi, R., Uchida, Y., 2007. Development of suitability maps for ground-coupled heat pump systems using groundwater and heat transport models. Geothermics 36, 459–472. https://doi.org/10.1016/j.geothermics.2007.06.002

Haehnlein, S., Bayer, P., Blum, P., 2010. International legal status of the use of shallow geothermal energy. Renew. Sustain. Energy Rev. 14, 2611–2625. https://doi.org/10.1016/j.rser.2010.07.069

Lo Russo, S., Civita, M.V., 2009. Open-loop groundwater heat pumps development for large buildings: A case study. Geothermics 38, 335–345. https://doi.org/10.1016/j.geothermics.2008.12.009

Lo Russo, S., Gnavi, L., Roccia, E., Taddia, G., Verda, V., 2014. Groundwater Heat Pump (GWHP) system modeling and Thermal Affected Zone (TAZ) prediction reliability: Influence of temporal variations in flow discharge and injection temperature. Geothermics 51, 103–112. https://doi.org/10.1016/j.geothermics.2013.10.008

Lund, J.W., Freeston, D.H., Boyd, T.L., 2011. Direct utilization of geothermal energy 2010 worldwide review. Geothermics 40, 159–180. https://doi.org/10.1016/j.geothermics.2011.07.004

Meng, B., Vienken, T., Kolditz, O., Shao, H., 2019. Evaluating the thermal impacts and sustainability of intensive shallow geothermal utilization on a neighborhood scale: Lessons learned from a case study. Energy Convers. Manag. 199, 111913. https://doi.org/10.1016/j.enconman.2019.111913

Nam, Y., Ooka, R., Hwang, S., 2008. Development of a numerical model to predict heat exchange rates for a ground-source heat pump system. Energy Build. 40, 2133–2140. https://doi.org/10.1016/j.enbuild.2008.06.004

Neton, M.J., Dorsch, J., Olson, C.D., Young, S.C., 1994. Architecture and directional scales of heterogeneity in alluvial-fan aquifers. J. Sediment. Res. B Stratigr. Glob. Stud. 245–257. https://doi.org/10.1016/0148-9062(94)90102-3

Ohtani, T., Mizuno, T., Kouda, A., Kojima, S., 2015. Seasonal Change of Underground Temperature and the Use of Geothermal in Gifu City ,. World Geotherm. Congr. 2015 19–25.

Okano, O., Konishi, A., Kita, A., Ueda, A., 2021. Geochemical study for utilization of groundwater heat by open heat pump system in northern Okayama and Akaiwa city areas with low precipitation in Japan. Groundw. Sustain. Dev. 12, 100494. https://doi.org/10.1016/j.gsd.2020.100494

Piga, B., Casasso, A., Pace, F., Godio, A., Sethi, R., 2017. Thermal impact assessment of groundwater heat pumps (GWHPs): Rigorous vs. simplified models. Energies 10. https://doi.org/10.3390/en10091385

Pophillat, W., Bayer, P., Teyssier, E., Blum, P., Attard, G., 2020. Impact of groundwater heat pump systems on subsurface temperature under variable advection, conduction and dispersion. Geothermics 83, 101721. https://doi.org/10.1016/j.geothermics.2019.101721

Rivoire, M., Casasso, A., Piga, B., Sethi, R., 2018. Assessment of energetic, economic and environmental performance of ground-coupled heat pumps. Energies 11. https://doi.org/10.3390/en11081941

Russo, S. Lo, Taddia, G., Baccino, G., Verda, V., 2011. Different design scenarios related to an open loop groundwater heat pump in a large building: Impact on subsurface and primary energy consumption. Energy Build. 43, 347–357. https://doi.org/10.1016/j.enbuild.2010.09.026

Sanner, B., Karytsas, C., Mendrinos, D., Rybach, L., 2003. Current status of ground source heat pumps and underground thermal energy storage in Europe. Geothermics 32, 579–588. https://doi.org/10.1016/S0375-6505(03)00060-9

Shrestha, G., Uchida, Y., Yoshioka, M., Fujii, H., Ioka, S., 2015. Assessment of development potential of ground-coupled heat pump system in Tsugaru Plain, Japan. Renew. Energy

76, 249–257. https://doi.org/10.1016/j.renene.2014.11.031

Sommer, W.T., Doornenbal, P.J., Drijver, B.C., van Gaans, P.F.M., Leusbrock, I., Grotenhuis, J.T.C., Rijnaarts, H.H.M., 2014. Thermal performance and heat transport in aquifer thermal energy storage. Hydrogeol. J. 22, 263–279. https://doi.org/10.1007/s10040-013-1066-0

Uchida, Y., Sakura, Y., Taniguchi, M., 2003. Shallow subsurface thermal regimes in major plains in Japan with reference to recent surface warming. Phys. Chem. Earth 28, 457–466. https://doi.org/10.1016/S1474-7065(03)00065-2

Yasukawa, K., Takasugi, S., 2003. Present status of underground thermal utilization in Japan. Geothermics 32, 609–618. https://doi.org/10.1016/j.geothermics.2003.07.011